PERGAMON

Journal of Structural Geology 25 (2003) 1371–1391

JOURNAL OF STRUCTURAL GEOLOGY

www.elsevier.com/locate/jsg

Texture, microstructure, and strength of hematite ores experimentally deformed in the temperature range 600–1100 °C and at strain rates between 10^{-4} and 10^{-6} s^{-1}

Heinrich Siemes[a,*], Birgit Klingenberg[a], Erik Rybacki[b], Michael Naumann[b], Wolfgang Schäfer[c], Ekkehard Jansen[c], Carlos A. Rosière[d]

[a]*Institut für Mineralogie und Lagerstättenlehre, RWTH Aachen, Wüllnerstr. 2, D-52056 Aachen, Germany*
[b]*Geoforschungszentrum Potsdam, Telegrafenberg, D-14473 Potsdam, Germany*
[c]*Mineralogisches Institut Bonn, Forschungszentrum Jülich, D-52425 Jülich, Germany*
[d]*Instituto de Geosciências, Universidade Federal de Minas Gerais, Av. Antonio Carlos 6627, CEP 31270-901 Belo Horizonte, MG, Brazil*

Received 21 April 2002; received in revised form 15 October 2002; accepted 1 November 2002

Abstract

Polycrystalline hematite samples cored perpendicular and parallel to the foliation, i.e. perpendicular and parallel to a weak c-axis maximum, respectively, were deformed in triaxial compression experiments at confining pressures of 300 and 400 MPa, temperatures T between 600 and 1100 °C, and strain rates between 10^{-4} and 10^{-6} s^{-1}. The measured strength of hematite ranges from 890 to 67 MPa.

The grain size of the main starting material is up to 175 μm. Grain boundaries are intensely serrated. At $T \leq 800$ °C the grain boundaries become increasingly lobate and the number of r-twins decreases. Dynamic recrystallization starts above 800 °C and a foam structure with grain sizes up to 150 μm develops at $T \geq 900$ °C.

Neutron diffraction measurements show a distinct change of the preferred orientation (texture) in compression parallel to the foliation. Below 800 °C a {300}-maximum developed due to {a}⟨m⟩ slip. At 800 and 900 °C a c-axis maximum evolved, probably due to (c)⟨a⟩ slip. The original texture is preferentially preserved but with lower densities at $T \geq 1000$ °C, presumably caused by increasing diffusional flow processes. Perpendicular to the foliation only minor changes of the texture occurred.

The experimentally determined textures allow a better understanding of the natural preferred orientation of hematite ores. The extrapolation of experimental strength data of hematite, quartz, and carbonates to geological conditions are compatible with field observations.

Keywords: Hematite ore; Experimental deformation; Recrystallization; Texture; Microstructure; Power law creep

1. Introduction

The relationship between the microstructure and texture (crystallographic preferred orientation) of hematite ores and the geological environment and deformation history of ore deposits, especially of ores from the Quadrilátero Ferrífero (Iron Quadrangle) in Minas Gerais, Brazil, has been the topic of a number of publications. Earlier papers (e.g. Rosière et al., 1996, 1998) studied the textures of hematite ores using pole figures measured by means of X-ray diffraction. More recent interpretations (e.g. Quade et al., 2000; Siemes et al., 2000; Rosière et al., 2001) are based on neutron diffraction pole figures, especially due to the capability of direct measurement of the basal plane even on large samples.

The c-axes of hematite from naturally deformed ores are concentrated in circular to elliptical maxima, and the long axis of the latter may be elongated to almost great circle distributions. The poles of all the prism planes lie on great circles with elliptical to circular concentrations perpendicular to the c-axes. These textures are interpreted as c-axis concentrations with rotational freedom of the a-axes around the c-axis (Siemes and Hennig-Michaeli, 1985; Will et al., 1990; Wenk, 1998). The c-axis maxima are centered on the pole of the foliation and all the prism

* Corresponding author. Fax: +49-241-8092153.
E-mail address: siemes@rwth-aachen.de (H. Siemes).

0191-8141/03/$ - see front matter © 2003 Elsevier Science Ltd. All rights reserved.
PII: S0191-8141(02)00184-0

maxima are centered on the lineation. As an example, the textures of two hematite ores from the Brucutu Mine (42°22′W,19°52′S), Iron Quadrangle, Minas Gerais, Brazil, are shown in Fig. 1. The Brucutu Mine is situated in the eastern high strain domain, cummingtonite zone of the Iron Quadrangle, which was "formed during one long lasting metamorphic stage in which temperature did not considerably change, being restricted in the range 300 and 600 °C" (Pires, 1995). The high densities of the pole figures in Fig. 1a belong to a sample from a highly deformed section of the mine, whereas the pole figures in Fig. 1b belong to a less deformed section. The formation of these textures, partially attributed to simple shear, and the relationship to the microstructures of the ores, is discussed in detail by Rosière et al. (2001).

It is postulated that the significant relationship between foliation and preferred orientation of the basal plane must be due to slip mechanisms in the basal plane which are not yet verified by deformation experiments. The principal objectives of the present experimental deformation tests are the analysis of the development of the preferred orientation and microstructure of hematite depending on temperature and strain rate and an attempt to correlate the experimental results with field observations.

2. Previous experimental work

The first systematic series of deformation experiments on hematite ores at low temperatures were performed by Hennig-Michaeli (1977). Compression experiments on coarse-grained ores from Malmberget, Lapland, Sweden, were run at strain rates between 10^{-4} and $10^{-5}\,s^{-1}$, temperatures of 25 and 450 °C and 400 and 600 MPa confining pressure. The optically identified deformation mechanisms were micro-fracturing, r-twinning and c-twinning. These qualitatively known mechanisms (Veit, 1922) were quantified by deformation experiments on single crystals of hematite (Hennig-Michaeli and Siemes, 1982). In addition to the twinning systems the slip system a$\{11\bar{2}0\}$m$\langle 1\bar{1}00\rangle$ was observed (Table 1).

Deformation experiments on synthetic polycrystalline Fe_2O_3 at high temperatures were performed by Crouch (1972, 1973) and Pascoe (1974). They used isostatically pressed and sintered (IPS) or hot pressed and heat treated (HP) hematite yielding final grain sizes of 1.5–35 μm with a porosity between 3 and 31 vol%. Crouch (1972) observed in compression tests (IPS and HP hematite) at strain rates ($\dot{\epsilon}$) between 10^{-4} and $10^{-7}\,s^{-1}$ and stresses (σ) between 10 and 80 MPa, a stress exponent (n, $\dot{\epsilon} \propto \sigma^n$) of 1.17 and in

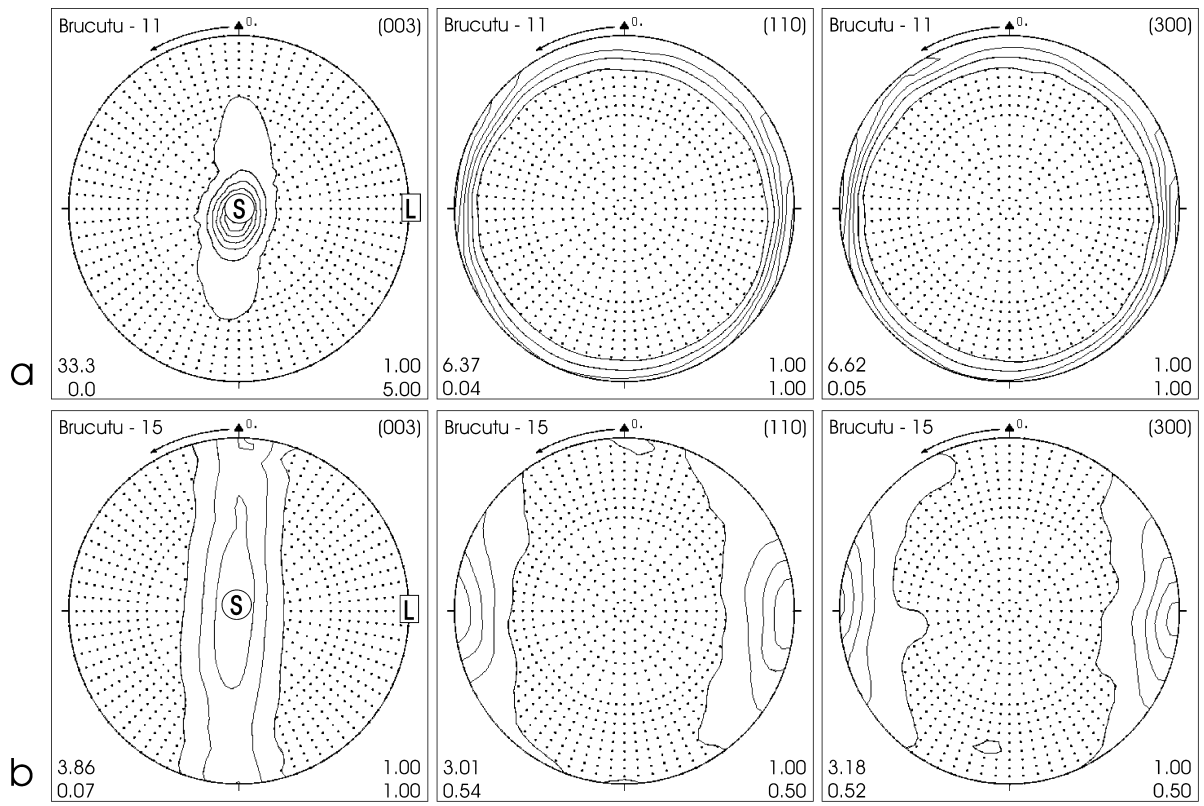

Fig. 1. Neutron pole figures of hematite ores from the Brucutu Mine, Iron Quadrangle, Brazil. Upper row: (003)-, {110}- and {300}-pole figures of a strong c-axis maximum centered on the pole of the foliation (S) associated with great circle distributions of the prism planes showing a maximum centered on the lineation (L). Lower row: (003)-, {110}- and {300}-pole figures of a weak elongated c-axis maximum centered on the pole of the foliation (S) associated with maxima of the prism planes centered on the lineation (L). All pole figures are equal area projections. In the lower left corner of the figures are indicated the maximum and minimum densities, in the lower right corner the first contour line and the contour intervals. The dotted area is below 1.0 m.r.d. (multiples of random density).

Table 1
Experimentally derived low temperature glide systems in hematite (Hennig-Michaeli and Siemes, 1982)

Fe_2O_3, trigonal corundum structure 400 MPa confining pressure	Strain rate	Temperature		crss[a]
	(s^{-1})	(°C)	(T/T_M)[b]	(MPa)
Hematite crystals, Ouro Preto, Brazil				
r{01$\bar{1}$2} ⟨01$\bar{1}\bar{1}$⟩ twinning	10^{-5}	25	0.16	140
K2 = {0$\bar{1}$14}		400	0.37	22
c{0001} ⟨0110⟩ twinning	2×10^{-5}	25	0.16	90
K2 = {0$\bar{1}$11}		400	0.37	>440
a{11$\bar{2}$0} m⟨1$\bar{1}$00⟩ slip	3×10^{-5}	25	0.16	>560
		200	0.26	370
		400	0.37	170
Comparison with Al_2O_3 data[c] suggests:				
c{0001} a⟨11$\bar{2}$0⟩ slip		>400		?

[a] crss = critical resolved shear stress.
[b] T_M, melting temperature Fe_2O_3: 1840 K, Al_2O_3: 2320 K.
[c] See references in Heuer et al. (1980) and Hennig-Michaeli and Siemes (1982). Stevenson et al. (2002) state that the room temperature microhardness anisotropy in the basal plane of hematite is associated with the dominance of the (c)⟨a⟩ slip.

bending tests (HP hematite) at strain rates between 10^{-4} and 10^{-9} s^{-1} and stresses between 1.5 and 45 MPa, with stress exponents between 1 and 2.2. Bending tests on IPS hematite at strain rates between 10^{-5} and 10^{-7} s^{-1} and low stresses (2 to approximately 20 MPa) yielded stress exponents of 1.14 to 1.19, and at higher stresses (approximately 20–40 MPa) stress exponents between 3.2 and 3.5. For the stress exponents close to one, he concluded that the dominant deformation mechanism in Fe_2O_3 at 900–1100 °C is Nabarro-Herring creep (lattice diffusion) accompanied by some grain boundary sliding. The stress exponents of approximately three are attributed to the operation of dislocation mechanism. These results were confirmed by tensile deformation tests (Crouch, 1973) and stress relaxation tests (Pascoe, 1974). No measurements of preferred orientation of hematite were performed in the course of Crouch's experiments.

Atkinson (1977) constructed a deformation mechanism map with normalized grain sizes versus normalized shear stresses and Frost and Ashby (1982) drew a deformation map (see Section 4.1) with normalized shear stresses versus temperatures. Both authors made use of the data of Crouch (1972) and concluded that the dominant mechanism in Crouch's experiments was Coble creep (grain boundary diffusion) rather than Nabarro-Herring creep.

3. Experimental methods and starting material

3.1. Starting material

As starting material a block of hematite ore from the Sishen Mine (23°E, 27°48′S), Postmasburg district, Northern Cape Province, South Africa was used. The Sishen Mine (Beukes, 1986) belongs to the banded iron formation of the Transvaal Supergroup with supergene enriched hematite. The modal composition of the starting material measured on polished sections and thin sections is 99.5% hematite and 0.5% quartz. X-ray and neutron diffraction measurement showed only very minor traces of magnetite. The faintly visible lamination is caused by alternating layers (thickness 200–1000 μm) of fine-grained (5–60 μm) and coarse-grained hematite (90–150 μm) with serrated grain boundaries (Fig. 2). From this hand-specimen 21 cylinders of 10 mm diameter and 20 mm length were cored in three orientations perpendicular to each other. The letter S indicates cylinders perpendicular to the foliation, N and P indicate cylinders parallel to the foliation. Because there was no lineation detectable in the foliation plane, the N and P cylinders are arbitrarily oriented parallel to the foliation but perpendicular to each other.

The texture of 13 undeformed samples were measured by neutron diffraction. The pole figures of samples in the same orientation show only minor differences (Table 2). The mean pole figures for the most important N-cylinders cored perpendicular to the foliation are shown in Fig. 3. The initial preferred orientation reveals a circular fiber texture with a c-axis maximum centered on the pole of the layering and weak great circle girdle distributions of the prism planes.

In addition some samples were cored from a block from ore from the Mutuca Mine (43°55′W, 20°02′S), Iron Quadrangle, Minas Gerais, Brazil. The Mutuca Mine is situated in the cummingtonite metamorphic zone under

Table 2
The range of maximum densities in single pole figures of undeformed hematite. S = Sishen ore and R = Mutuca ore perpendicular to foliation, N and P = Sishen ore parallel to foliation

	S-cylinders:	N-cylinders	P-cylinders	R-cylinders
(003):	1.75–1.95	1.98–2.16	2.14	2.00
{104}:	1.17–1.21	1.21–1.25	1.28	1.21
{110}:	1.26–1.31	1.23–1.32	1.25	1.25
{300}:	1.19–1.27	1.19–1.30	1.49	1.23

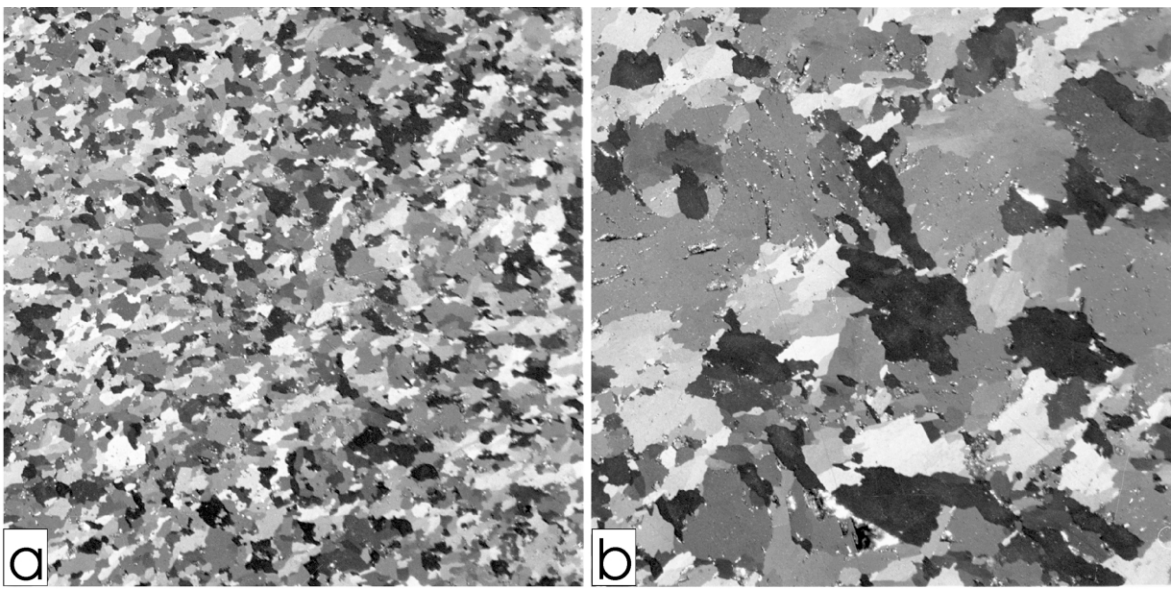

Fig. 2. Photomicrographs of the hematite ore from Sishen Mine. Polished section perpendicular to the foliation, 87° XPL; width of view 600 μm: (a) sector with preferentially small grains between <5 and 65 μm, (b) sector with preferentially large grains between 90 and 175 μm.

similar temperatures as the Brucutu Mine, but much lower strain conditions. The microfabric and the preferred orientation is similar to the ore from Sishen Mine, but the grain size is slightly larger, the grain boundaries are lobate, the quartz content is somewhat lower and magnetite content somewhat higher (<1%), and a minor amount of other silicate minerals is present. The cylinders were cored parallel to the foliation in order to increase the number of samples for the texture interpretation. These are denoted as R-samples.

For comparison with hematite two tests on a magnetite ore from Graengesberg (60°06′E, 15°N), Dalarnas län, Sweden, were run (see Section 4.1). The ore consists of about 95% magnetite with grain sizes between 5 and 20 μm separated by apatite, phlogopite and traces of other silicates.

3.2. Deformation apparatus and experimental procedure

The samples were deformed in compression tests using a high resolution Paterson-type gas-medium apparatus (Paterson, 1970, 1990). They are separated from the confining pressure medium argon by iron jackets with a wall thickness of 0.34 mm, i.e. buffered to an iron–wuestite environment. The data from force-displacement records were used to calculate the stress and strain curves assuming constant volume, corrected for the strength of the iron-jacket, and for the apparatus compliance.

The maximum capacity of the loading system in relation to the strength of hematite permitted tests down to 700 °C at strain rates up to $10^{-4}\,s^{-1}$. At a strain rate as low as $10^{-6}\,s^{-1}$ tests could be run at 600 °C. From preliminary tests in Canberra it is known that under experimental conditions the iron-jacket reacts with the hematite samples to form cubic magnetite (Fe_3O_4) and cubic wuestite (FeO). Using copper as the jacket material resulted in a rim of wuestite and minor trigonal delafossite ($CuFeO_2$) (Hennig-Michaeli, pers. comm., 1991). Therefore, in the present

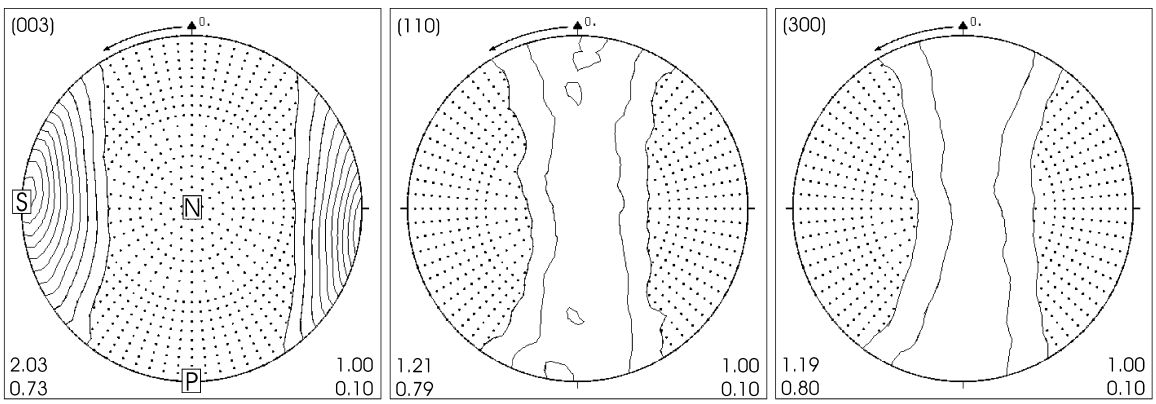

Fig. 3. Neutron pole figures of undeformed hematite (Sishen Mine) perpendicular to the foliation. S,N,P are the axes of the cored cylinders. The circular (003)-maximum is concentrated on the pole of the foliation (S). {110}- and {300}-pole figures show great circle distributions with a very weak higher intensity of {110} close to the P-axis.

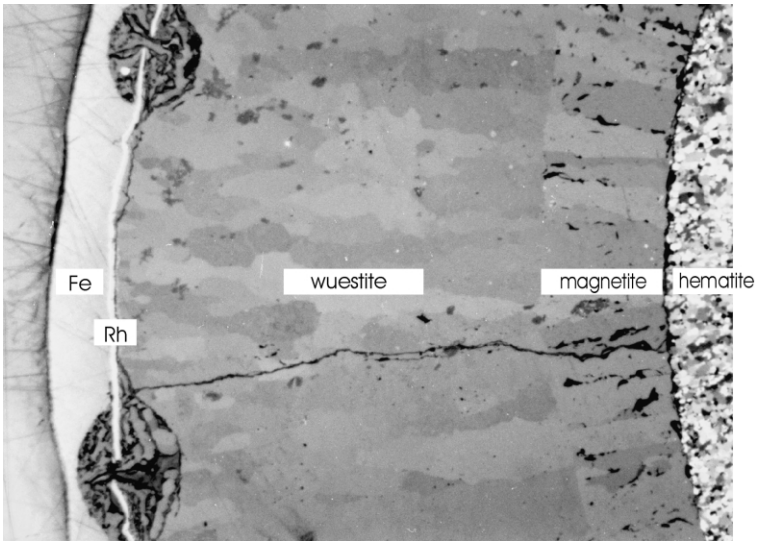

Fig. 4. Photomicrograph of the formation of magnetite and wuestite as reaction product between Fe-jacket and Fe_2O_3-sample. Polished section perpendicular to the long axis of the cylinder N11 deformed at 1070 °C, width of view 2400 μm. From right to left: hematite, magnetite (~440 μm), wuestite (~1460 μm), rhenium foil (20 μm) with cracks, and iron jacket (~220 μm, original thickness 340 μm). At the cracks in the rhenium foil an intense reaction with the iron jacket occurred.

experiments different foils (gold, rhenium, silver/palladium alloy) were placed in between iron-jacket and sample in order to prevent or at least to minimize reaction products. As an example for the formation of the reaction products during deformation Fig. 4 shows a cross-section of a specimen with rhenium as separating foil.

A foil of silver(70)–palladium(30) alloy of 20 μm thickness was most efficient. A material that was used for sample containers in petrological experiments in order to prevent Fe loss to the containers from partially molten lherzolite (Kawamoto and Hirose, 1994; Hirose and Kawamoto, 1995). In tests of 1680 min duration at 600 and 700 °C wuestite could not be detected, and the reaction to magnetite was significantly reduced yielding a rim thickness of only 30 μm at 600 °C, 60 μm at 700 °C, and a maximum of 300 μm at 950 °C. Strength values of the silver/palladium alloy are not available. However, comparison of the room temperature strength of silver (172 MPa) and palladium (140–194 MPa) with iron (180–210 MPa) makes it reasonable to assume to a first order approximation that at high temperatures the Ag/Pd-foil has a comparable strength with the iron of the jacket. This assumption is confirmed by data calculations (Frost and Ashby, 1982), which show comparable strengths for silver and iron, and by the fact that Palladium has a strength of only 8.1 MPa at 1300 °C (Fischer and Helmich, 1981).

3.3. Neutron diffraction texture measurement

The complete pole figures representing textures of undeformed and experimentally deformed ore cylinders were measured using a neutron texture-diffractometer (SV7; Jansen et al., 2000) at the Research Center Jülich, Germany. Since this texture diffractometer is equipped with a position sensitive detector the reflections of all mineral components (hematite, magnetite, wuestite, quartz, carbonates) over a 2Θ-range of 50° using a wavelength of 1.20 Å could be measured in one scan. The standard scan grid comprises about 500 sample positions and needs a measuring time of about 20 h. A few pole figures were obtained with a neutron goniometer (TEX2; Brokmeier et al., 1998) at the Research Center GKSS, Geesthacht, Germany. A short description of the advantages of neutron diffraction in relation to X-ray diffraction for texture analysis is given by Rosière et al. (2001), very detailed descriptions are given for example by Bunge (1989) and Brokmeier (1994, 1999).

The most suitable high intensity reflections for the interpretation of the textures of trigonal hematite and the comparison with published pole figures are (003), {110}, {300} and {104}. The MENTEX-program (Schaeben, 1994; Schaeben and Siemes, 1996) was used to calculate unmeasured pole figures. For example, the secondary phases magnetite and wuestite have some interesting reflections that coincide with hematite reflections. The {111}-peak of magnetite and (003) of hematite overlap and the{110}-peak of hematite, the {311} of magnetite, and {111} of wuestite cannot be separated and have to be calculated from other measured pole figures. All pole figures are smoothed (Traas et al., 1994) and plotted in equal area projections with the compression axis perpendicular to the projection plane.

4. Experimental results

4.1. Strength of the samples

In total 23 samples were deformed at constant displacement

Table 3
Experimental deformation of polycrystalline hematite in constant strain rate compression tests with gold and rhenium as separating foils

Specimen-no. & jacket[a]	Temperature		$\dot{\epsilon}$	$\Delta\sigma$ (MPa)			ϵ_{max}	$\Delta\sigma_{max}$	$\epsilon_{\Delta\sigma max}$	Test duration	Rim thickness	μm magnetite	Conf. press.
	(°C)	(T/T_M)[b]	(s^{-1})	($\epsilon_{5\%}$)	($\epsilon_{10\%}$)	($\epsilon_{max\%}$)	(%)	(MPa)	(%)	(min)	(total)		(MPa)
N01 cu[c]	800	0.58	10^{-5}	421.	384.	365	12.5	421.	4.7				300
S01 fe[c]	770	0.57	10^{-5}	387.	362.	351.	12.3	391.	3.8				300
S02 cu[c]	1000	0.69	10^{-5}	46.	53	53	10.7	54.	10.5				300
N02 au	700	0.53	10^{-4}	653.	662.	640.	14.5	665.	9.3	34	−80	+[d]	300
N04 au	800	0.58	10^{-4}	400.	383.	328.	21.0	402.	3.9	42	170–220	40	300
S04 au	800	0.58	10^{-4}	403.	393.	352.	20.6	404.	5.5	41	185–220	+	300
N05 au	900	0.64	10^{-4}	239.	226.	210.	20.5	242.	3.7	41	260–300	50	300
N03 au	1000	0.69	10^{-4}	108.	102.	94.	20.9	111.	2.9	39	500–960	130	300
N06 au	1100	0.74	10^{-4}	43.	41.	38.	20.4	44.	5.6	38	−2100	250	300
S06 au	900	0.64	10^{-5}	87.	80.	69.	20.5	94.	3.4	360	1100–1360	130	300
N12 re	700	0.53	10^{-4}	770.	738.	700.	21.5	785.	9.0	56	−30	−30	300
N07 re	1000	0.69	10^{-4}	180.	173.	168.	16.1	184.	3.0	28	260–300	50	300
S03 re	700	0.53	10^{-5}	587.	586.	541.	21.3	591.	8.1	420	−50	−50	300
N08 re	700	0.53	10^{-5}	650.	638.	560.	21.1	652.	5.2	380	30–50	30–50	300
N13 re	800	0.58	10^{-5}	313.	285.	245.	21.7	324.	3.2	420	120–135	120–135	300
N14 re	900	0.64	10^{-5}	161.	151.	141.	21.0	166.	2.8	360	300–350	+	300
S08 re	1000	0.69	10^{-5}	60.			(20.0)	63.[e]	2.8	340	550–580	+	300
N11 re	1070	0.72	10^{-5}	40.	32.	20.	15.5	46.[f]	2.1	xxx	>1400	>440	300

[a] S = test cylinders of Sishen ore perpendicular to the foliation, N,P = test cylinders of Sishen ore parallel to the foliation iron-jacket with: au = gold foil 6 μm, re = rhenium 20 μm thickness.
[b] T_M = melting temperature 1840 K.
[c] Preliminary tests in Canberra.
[d] + = magnetite rim present, but not measured.
[e] Failure of the jacket above 5% strain.
[f] Specimen stayed more than 8 h at temperatures above 950 °C.

Table 4
Experimental deformation of polycrystalline hematite in step strain rate and constant strain rate compression tests with silver/palladium as separating foils

Specimen jacket[a]	Temperature		$\dot{\epsilon}$	$\Delta\sigma_{(step)}$	ϵ_{max}	Test duration	Magnet.	Conf. press.	$\log_{10}$	$\Delta\log_{10}$	$\Delta\log_{10}$	$n =$
	(°C)	(T/T_M)[b]	(s^{-1})	(MPa)	(%)	(min)	(μm)	(MPa)	(2)	(3)	(1)	(5)/(4)
			1	2					3	4	5	
R20 ag	600	0.47	10^{-6}	686.	7.1	1680	30	300	2.836			
R22 ag	700	0.53	10^{-6}	421.	8.3	1680	60	300	2.624			
P02 ag	700	0.53	10^{-6}	525.	11.0	900	+[c]	400	2.720			
			10^{-5}	740.					2.869	0.149	1	6.7
			10^{-4}	889.					2.949	0.080	1	12.5
N15 ag	800	0.58	10^{-6}	240.	12.4	900	200	400	2.380			
			10^{-5}	410.					2.613	0.233	1	4.3
			10^{-4}	553.					2.743	0.130	1	7.7
R19 ag	900	0.64	10^{-6}	112.	9.6	900	250	400	2.049			
			10^{-5}	260.					2.415	0.366	1	2.7
			10^{-4}	374.[d]					2.573	0.158	1	6.3
R24 ag	950	0.66	10^{-6}	67.	6.4	1060	300	370	1.826			
R21 ag			10^{-5}	158.	12.7	1090	+[c]		2.199	0.373	1	2.7
			10^{-4}	256.					2.408	0.209	1	4.8
P01 ag	1000	0.69	10^{-5}	48.[e]	8.9	220	200	400	1.681			

[a] R = test cylinders of Mutuca ore parallel, N,P = test cylinders of Sishen ore parallel to the foliation iron-jacket with: ag = silver(70)/palladium(30) foil 20 μm.
[b] T_M = melting temperature 1840 K.
[c] Magnetite rim present, but not measured.
[d] Fractured at the end of the test.
[e] Stress value is too low, strong formation of magnetite because of failure of the Ag/Pd-foil at the top of the specimen and failure of the jacket at 8.9% strain.

rates corresponding to strain rates of 10^{-4}–10^{-6} s^{-1} at temperatures between 600 and 1100 °C and a confining pressure of 300, 370 or 400 MPa (Tables 3 and 4). Usually the samples were strained up to 20% or more in order to achieve significant reordering of the texture. Lower strains usually indicate failure of the sample in the course of the test. The tests with strain rates of 10^{-6} s^{-1} at 600 and 700 °C were stopped after 7–8% strain. The tests with strain rate steps of 10^{-6}, 10^{-5} and 10^{-4} s^{-1} were performed on four samples at 700, 800, 900, and 950 °C with maximum strain of 12%. Because of the unknown influence of the strength of the gold and the rhenium foil as well as the unknown kinetics of the two phase rim development attempts to correct the data were not reliable. The strength data of hematite of the experiments documented in Table 3 are systematically underestimated values, and therefore, the deformed samples are only used for the interpretation of textures. In the remaining discussion of mechanical data we focus on samples deformed with the Ag/Pd as separating foil (Table 4). The resulting maximum stresses of these samples are between 890 MPa at 700 °C, $\dot{\epsilon}$ 10^{-4} s^{-1} and 67 MPa, at 950 °C, $\dot{\epsilon}$ 10^{-6} s^{-1}.

The correction of the raw data for the silver/palladium foil has been performed by an increase of the thickness of the iron jacket from 0.34 to 0.36 mm. For the thin magnetite rim any correction has been neglected because our two tests on magnetite (Table 5) show that the strength of magnetite is only up to 16% lower at 700 °C and up to 33% higher at 800 °C (compare Tables 4 and 5). Indentation hardness measurements of Kollenberg (1986) on single crystals of hematite and Charpentíer et al. (1968) on single crystals of magnetite indicate a Vickers hardness for both minerals between 100 and 200 at temperatures ≥600 °C. Fig. 5a shows the stress-strain curves for the compression tests on hematite with the Ag/Pd separating foil at a strain rate of 10^{-6} s^{-1} and temperatures of 600, 700, and 950 °C. Fig. 5b

Table 5
Experimental deformation of polycrystalline magnetite (Graengesberg, Sweden) in step strain rate compression tests

Specimen-no. & jacket[a]	Temperature (°C)	Strain rate (s^{-1})	$\Delta\sigma_{(max\ step)}$ (MPa)	ϵ_{max} (%)	Conf. press. (MPa)	$\Delta\sigma_{(hematite)}/\Delta\sigma_{(magnetite)}$
MG02 ag	700	10^{-6}	519.	11.8	400	0.99
		10^{-5}	666.			0.89
		10^{-4}	750.			0.84
MG01 ag	800	10^{-6}	322.	12.0	400	1.33
		10^{-5}	516.			1.26
		10^{-4}	675.			1.19

[a] Iron-jacket with: ag = silver(70)/palladium(30) foil 20 μm.

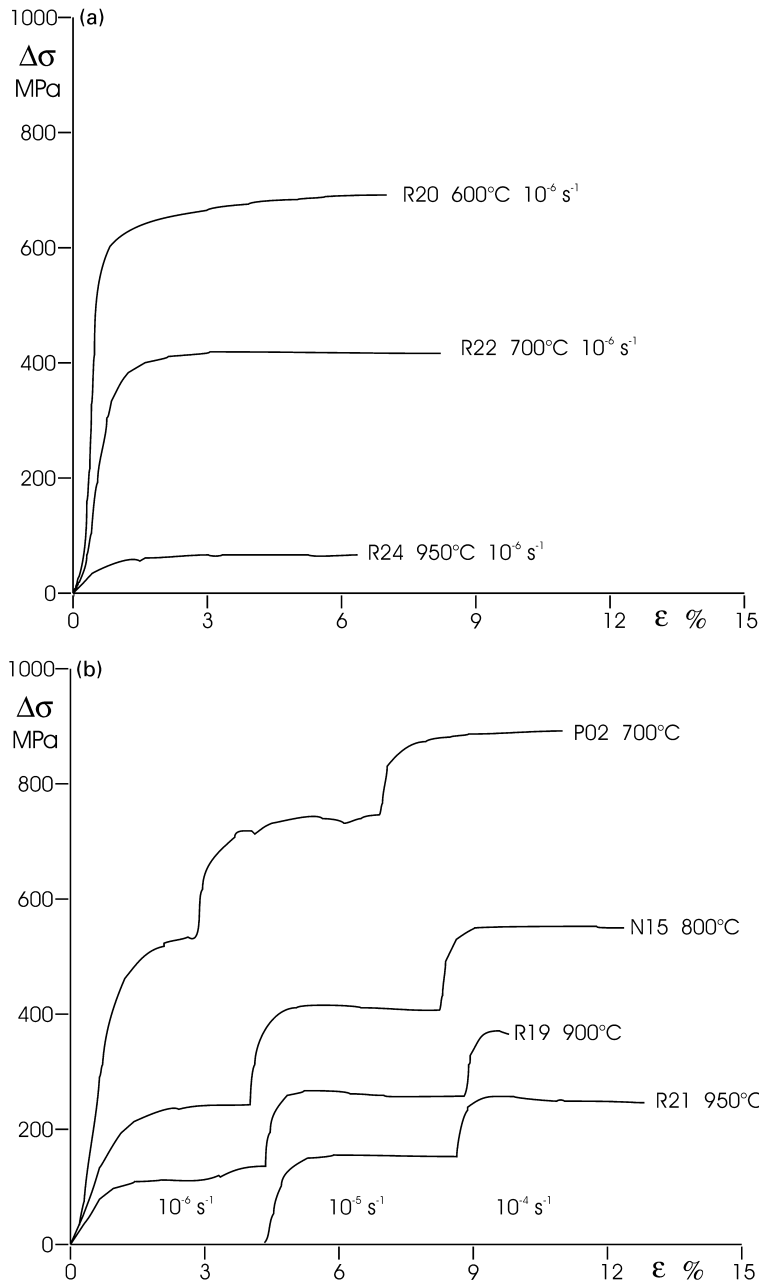

Fig. 5. Stress strain curves of the tests run with a separating foil of silver/palladium: (a) constant strain rate tests at a strain rate of 10^{-6} s^{-1} and 600, 700, and 950 °C temperature, (b) strain rate stepping tests at 10^{-6}, 10^{-5}, 10^{-4} s^{-1} and 700, 800, 900, and 950 °C. Sample numbers refer to Table 4.

shows strain rate stepping tests between 10^{-6} and 10^{-4} s^{-1} and temperatures between 700 and 950 °C. The difference in the stress-strain curves of the two tests (P02 and R22) at 700 °C/10^{-6} s^{-1} may be attributed to between sample variation of strength since both samples are from different localities. In addition, sample P02 (Sishen) was tested at a higher confining pressure of $p = 400$ MPa in comparison with sample R22 (Mutuca) which was deformed at $p = 300$ MPa. Therefore the fugacity (partial pressure) of oxygen was different leading to a somewhat different strength in agreement with the findings of Crouch (1972) and Chang and Wagner (1972). All data in Table 4 are presented in a $\log_{10}$ differential stress vs. $\log_{10}$ strain rate in Fig. 6. It is obvious from this figure that the orientation with respect to the foliation is subordinate compared with changes in strain rate and temperature. The calculated stress exponents n between two strain rate steps are indicated. The as yet still sparse data show a continuous decrease of the stress exponent n with increasing temperature and decreasing strain rate, possibly representing a continuous change of the relative contribution of dislocation glide and creep mechanisms and decreasing twinning activity (see Section 4.3).

The points in the hematite deformation map of Frost and

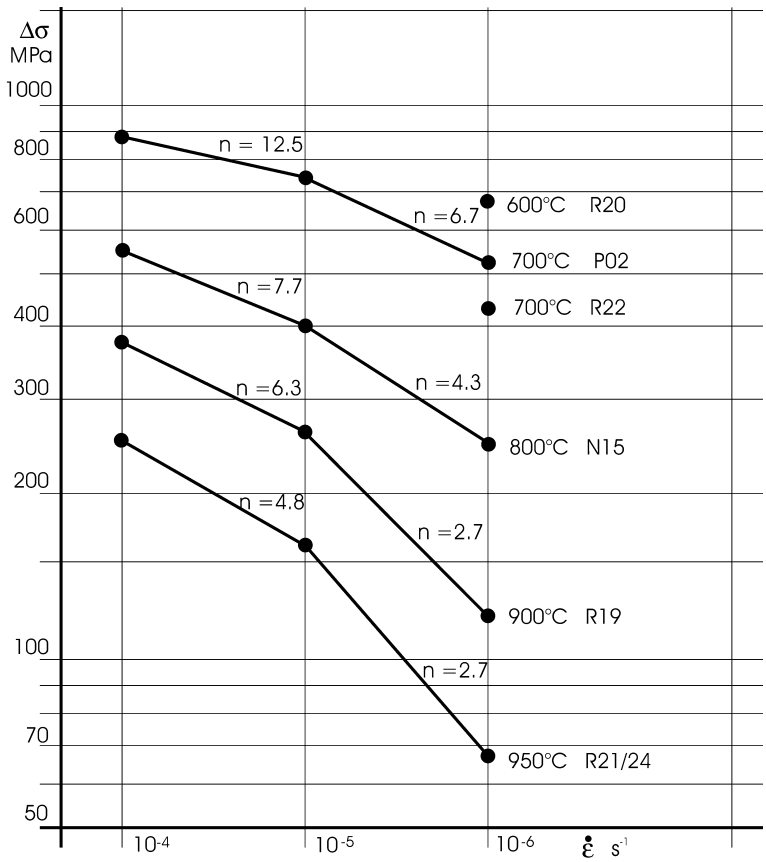

Fig. 6. Strain rate stepping and compression test data of Table 4 plotted as $\log_{10}$ differential stress vs. $\log_{10}$ strain rate. The stress exponents n between two steps are indicated.

Ashby (Fig. 7) show the positions of the experimental data recorded in Table 6. All data points are within the power law field, but with a considerable offset in relation to the strain rate contours of the map. The reason for the differences will be discussed in the last section. The experimental data of Table 4 were fitted using a generalized nonlinear matrix inversion (Sotin and Poirier, 1984) to the power law creep equation of the form $\dot{\epsilon} = A\sigma^n \exp(-Q/RT)$ where $\dot{\epsilon}$ is strain rate (s^{-1}), A is a pre-exponential constant ($MPa^{-n}\ s^{-1}$), σ is stress (MPa), Q is the activation energy (kJ mol^{-1}), T is temperature (K), R is the gas constant, and n the stress exponent. The most reliable values are

Table 6
Experimental stress data from Table 4 and extracted stress data from the hematite deformation map (Frost and Ashby, 1982)

Strain rate temperature	Experimental data (MPa)			Frost and Ashby data (MPa)			Ratio
(°C)	Normal stress	Shear stress	Normalized shear stress	Normalized shear stress	Shear stress	Normal stress	F&A data/exp. data
$\dot{\epsilon} = 10^{-4}\ s^{-1}$							
700	889	513	6.28×10^{-3}				
800	553	319	3.95×10^{-3}	7.88×10^{-3}	636	1102	1.99
900	374	216	2.70×10^{-3}	4.62×10^{-3}	369	638	1.70
950	256	148	1.86×10^{-3}	2.91×10^{-3}	231	400	1.56
$\dot{\epsilon} = 10^{-5}\ s^{-1}$							
700	740	427	5.23×10^{-3}	8.14×10^{-3}	666	1153	1.56
800	410	237	2.93×10^{-3}	5.40×10^{-3}	436	755	1.84
900	260	150	1.88×10^{-3}	2.47×10^{-3}	197	342	1.32
950	158	91	1.15×10^{-3}	1.55×10^{-3}	123	212	1.34
$\dot{\epsilon} = 10^{-6}\ s^{-1}$							
700	525	303	3.71×10^{-3}	5.53×10^{-3}	452	783	1.49
800	240	139	1.72×10^{-3}	3.35×10^{-3}	271	469	1.95
900	112	65	0.81×10^{-3}	1.34×10^{-3}	107	186	1.66
950	67	39	0.49×10^{-3}	0.85×10^{-3}	67	117	1.74

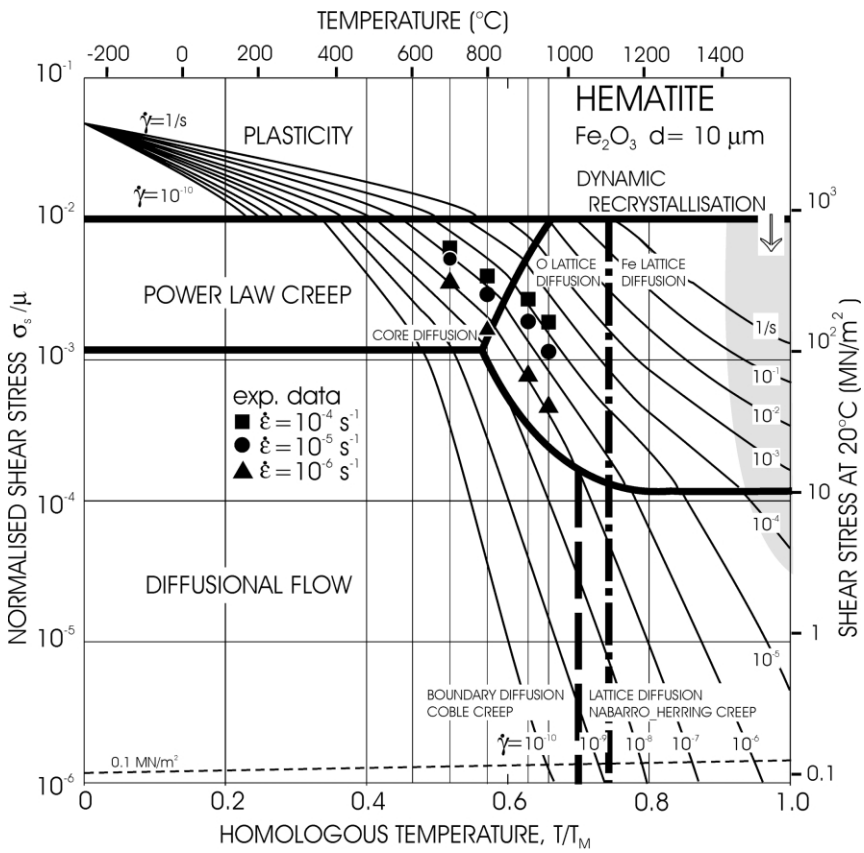

Fig. 7. Stress vs. temperature deformation map for hematite with a grain size of 10 µm (redrawn and supplemented fig. 14.7 of Frost and Ashby, 1982). The data of Table 4 are positioned in the map according to their calculated normalized shear stress vs. experimental temperature and labeled with different symbols for the experimental strain rate $\dot{\epsilon}$.

$\ln A = -9.5 \pm 1.3$ MPa^{-4} s^{-1}, $Q = 225 \pm 20$ kJ mol^{-1}, and $n = 4.0 \pm 0.3$, indicating dislocation creep as the main deformation mechanism.

4.2. Texture development of hematite

The most important changes of preferred orientations (Figs. 8–10) compared with the starting material (Fig. 3) occurred in samples cored parallel to the foliation (N, P, R). Depending on the deformation temperature there are three different preferentially developed patterns.

The first type (Fig. 8) shows that the prism girdles separate on the original girdle into three distinct maxima for strain rates of 10^{-4} and 10^{-5} s^{-1}. One of the three maxima of the {300}-pole figure is located in the center of the projection with a circular arrangement of the poles, and the other two elongated maxima are located on a small circle 60° from the center. Two of the {110}-maxima are located 30° symmetrically from the center, the third maximum is strongly elongated on a great circle. The (003)-pole figures show only minor changes with some elongation of the maximum to the center of the projection. In this orientation parallel to the foliation, i.e. perpendicular to the prisms in the prism girdles, there is a rotation of crystallites about the c-axis, which causes the {110}-maxima under 30° to the compression axis with rather high resolved shear stresses in these planes of the a{110}m$\langle 1\bar{1}0\rangle$ slip systems. All other known glide systems have low or zero resolved shear stresses. This pattern is well developed up to 700 °C and can be detected as a subordinate texture component at a temperature of 800 °C. The two tests at 600 and 700 °C and strain rates of 10^{-6} s^{-1}, which could be deformed only to 7.1 and 8.3%, respectively, do not show any indication of this pattern.

The second type (Fig. 9) is characterized by forming a central maximum of (003) and peripheral maxima of the {110}- and {300}-prisms at the same position on the periphery for strain rates of 10^{-4} and 10^{-5} s^{-1}. The development of this configuration may be due to a rotation of the crystallites by the basal glide system c(001) a$\langle 110\rangle$, which could be expected to operate analogous to the slip systems in corundum. This pattern prevails in the textures of the 800 °C experiments, but can be also detected at 700 °C. The transition from pattern 1 to pattern 2 is connected with the larger stress drop between 700 and 800 °C. As mentioned before there is already an indication of this pattern at 600 and 700 °C for the two tests at a strain rate of 10^{-6} s^{-1}.

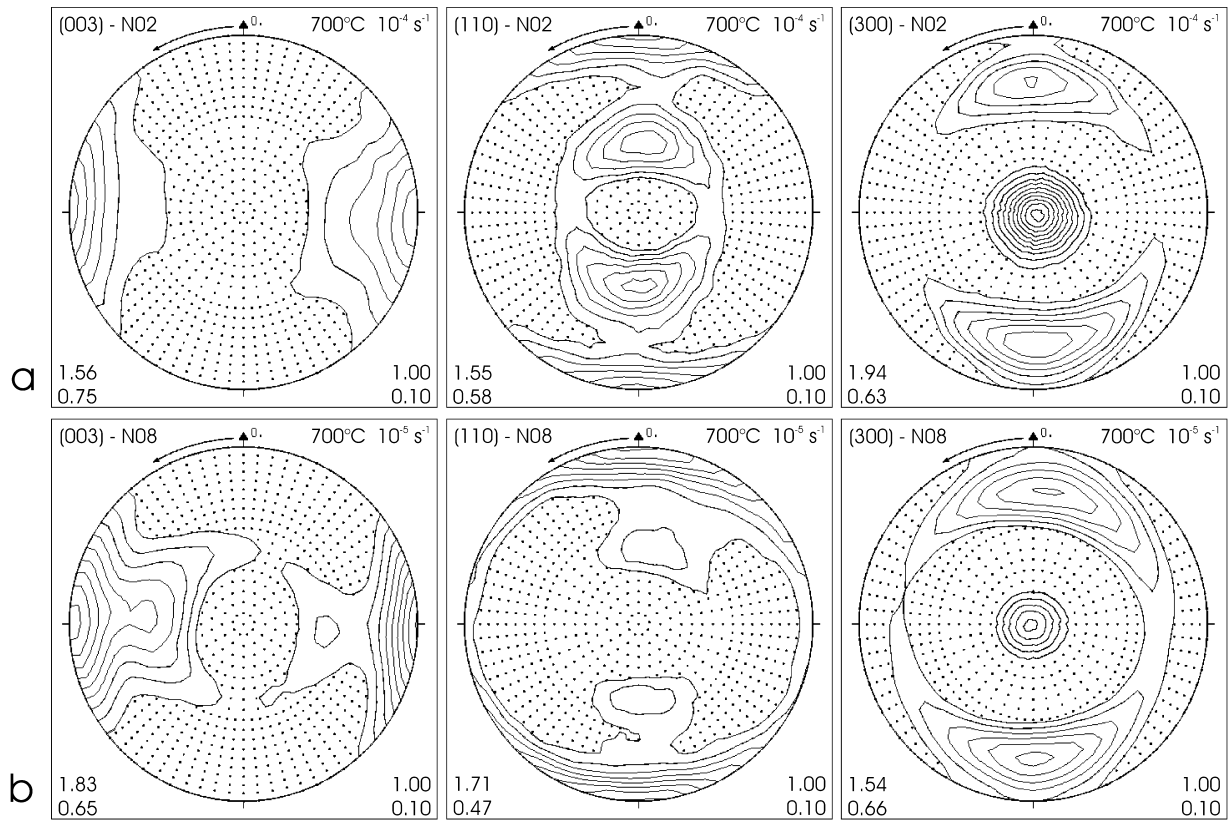

Fig. 8. (003)-, {110}- and {300}-Pole figures of experimentally deformed Sishen N-samples at temperatures of 700 °C: (a) specimen N02, 700 °C, $\epsilon = 14.5\%$, $\dot{\epsilon} = 10^{-4}\ s^{-1}$, (b) specimen N08, 700 °C, $\epsilon = 21.1\%$, $\dot{\epsilon} = 10^{-5}\ s^{-1}$.

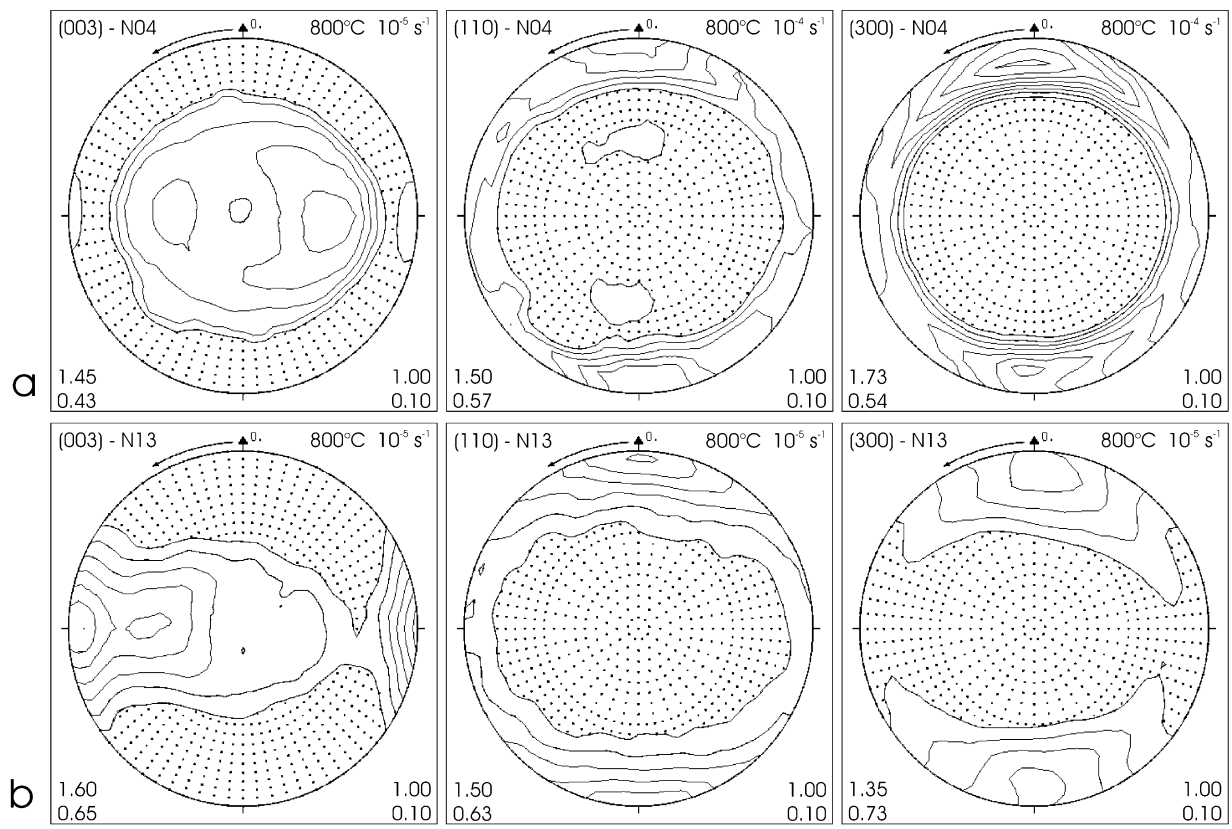

Fig. 9. (003)-, {110}- and {300}-Pole figures of experimentally deformed Sishen N-samples at temperatures of 800 °C: (a) specimen N04, 800 °C, $\epsilon = 21.0\%$, $\dot{\epsilon} = 10^{-4}\ s^{-1}$, (b) specimen N13, 800 °C, $\epsilon = 21.7\%$, $\dot{\epsilon} = 10^{-5}\ s^{-1}$.

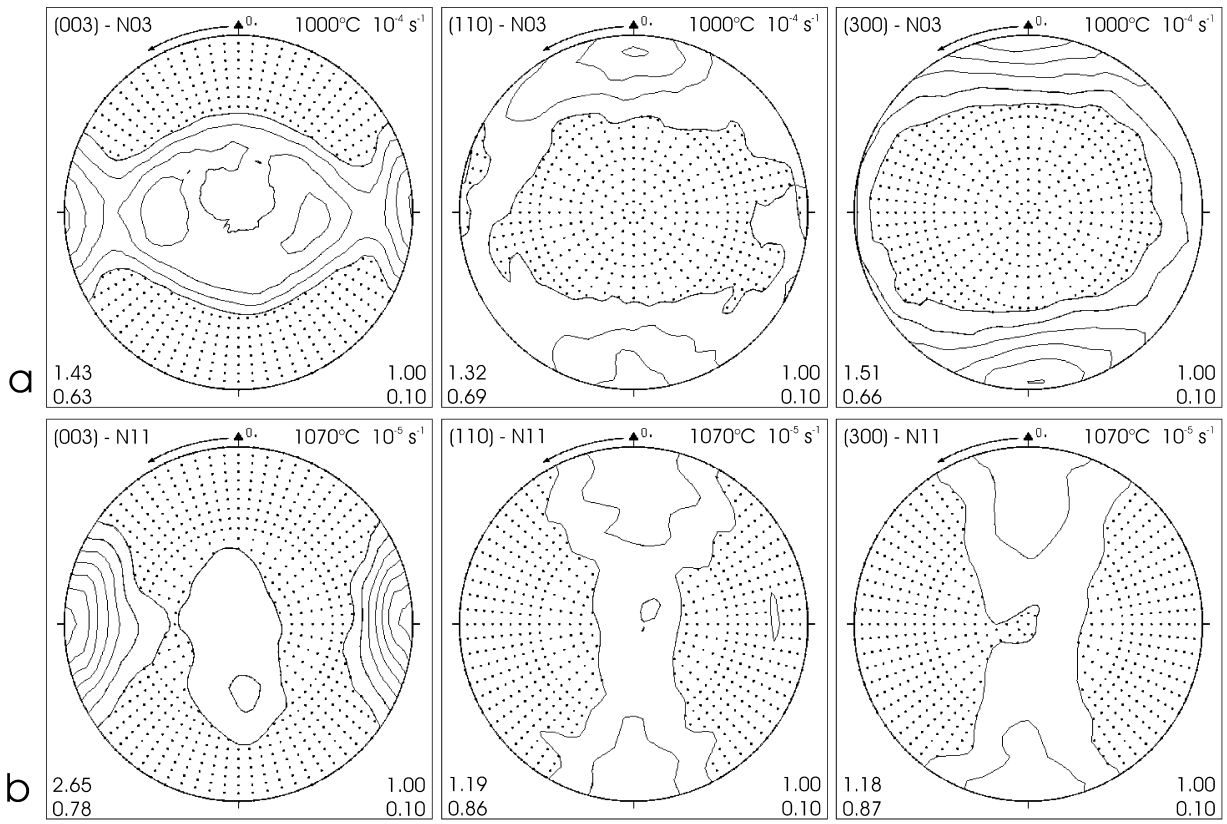

Fig. 10. (003)-, {110}- and {300}-Pole figures of experimentally deformed Sishen N-samples at temperatures of ≥1000 °C: (a) specimen N03, 1000 °C, $\epsilon = 20.9\%$, $\dot{\epsilon} = 10^{-4}\,s^{-1}$, (b) specimen N11, 1070 °C, $\epsilon = 15.5\%$, $\dot{\epsilon} = 10^{-5}\,s^{-1}$.

The third type (Fig. 10) is discernible in specimens deformed at the highest experimental temperatures (≥1000 °C) and the lowest strain rates. The original pattern of the undeformed samples is preserved but the densities are more or less lowered and a weak central (003)-maximum is visible. This pattern is due to the increase of diffusional flow processes. According to the deformation map (Fig. 7) these tests are rather close to the Coble creep field.

The pole figures of the strain-rate stepping tests show more or less distinct mixtures of these three patterns.

The textures of the S-cylinders cored perpendicular to the foliation underwent only minor but different changes in the density of the (003)-maxima depending on temperature. At lower temperatures the densities decrease and at higher temperatures they increase. Two examples are given in Fig. 11. An orientation with the c-axis parallel to the compression axis is most favorable for the initiation of r-twinning. This deformation mode induces a rotation of the c-axis of the twin lamellae to a position 64.7° apart from the c-axis of the parent crystal close to the pole of the {101}-plane. The other known mechanisms are in unfavorable orientations with respect to the compression axis. The r-twinning deformation mechanism may explain the lowering of the density of (003)-maxima at lower temperatures, but in the {101}-pole figures of the deformed S-samples no indication of a maximum in the center could be detected. The volume fraction of the twinned material is probably too small. The increase of (003)-maxima at higher temperatures is certainly due to the increasing influence of the (c) ⟨a⟩ slip system as described in the course of the interpretation of the deformation pattern of the N-cylinders.

A comparison of the hematite pole figures and the microstructures from tests with different separating foils reveals no significant differences from the ones that were run at the same temperature and strain rate.

4.3. Microstructure development of hematite

The grain size layering described in the starting material can still be observed under the microscope up to the highest testing temperatures. Fig. 12 shows a series of photomicrographs revealing areas of smaller and coarser crystal sizes at different testing temperatures between 700 and 1100 °C and a strain rate of $10^{-4}\,s^{-1}$. With increasing temperature the spectrum of the small grains changes from 5–60 μm (Fig. 12a left) to 25–60 μm (Fig. 12e left) and of the larger grains from 90–175 μm (Fig. 12a right) to 50–150 μm (Fig. 12e right). The originally intensely serrated grain boundaries become smoother and lobate (Fig. 12c) with the beginning of dynamic recrystallization. It is assumed that mainly subgrain boundary rotation leads to the development of subgrains indicated by undulose extinction and subgrain boundaries within the larger grains. With increasing temperature grain growth leads to a foam structure with

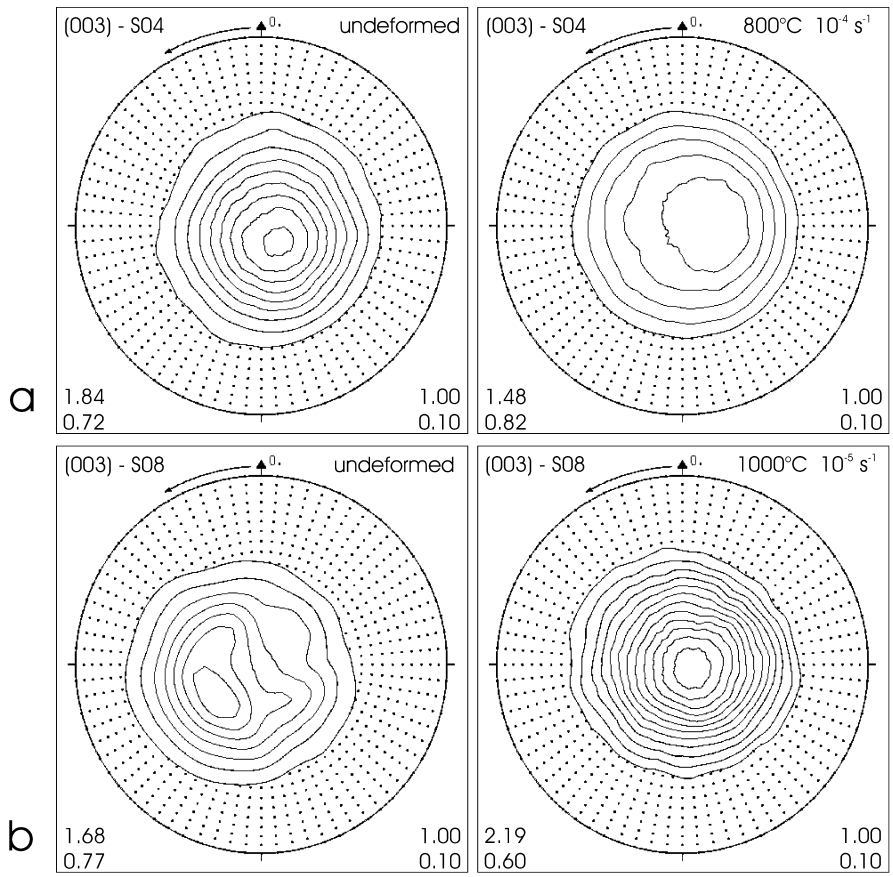

Fig. 11. (003)-Pole figures of Sishen S-samples before and after experimental deformation: (a) specimen S04 maximum density undeformed greater than maximum density after deformation at 800 °C, (b) specimen S08 maximum density undeformed lower than maximum density after deformation at 1000 °C.

smooth grain boundaries and a grain size from 20 to 50 μm (Fig. 12e).

The photomicrographs of Fig. 13a show the grain fabric of sample S06 deformed at a temperature of 900 °C and a strain rate of $10^{-5}\,s^{-1}$, which is quite similar to the microstructure of the specimen deformed at 1000 °C and $10^{-4}\,s^{-1}$ in Fig. 12d. The microstructures of the samples from the Mutuca Mine deformed at 600 and 700 °C at a strain rate of $10^{-6}\,s^{-1}$ (Fig. 13b) appear to have slightly smoother grain boundaries than the grain boundaries of the undeformed ore and more elongated grains than those in Fig. 12. Twinning, which partially accommodates strain in the large grains up to 800 °C (Fig. 12b), is almost absent at higher temperatures.

In the range of the studied temperatures and strain rates there is no distinct difference in the grain fabric between hematite samples deformed parallel and perpendicular to the foliation.

4.4. Texture and microstructure of magnetite and wuestite

The diffusion of iron from the jacket into the hematite sample yields a rim of magnetite and wuestite. Fig. 4 shows a growth texture with columnar cell structure of the grains of both phases with the long axes perpendicular to the iron jacket and the hematite core. In samples where the intensity of the magnetite and/or wuestite reflections are high enough a few pole figures were extracted. Three pole figures of wuestite (N06) and magnetite (S08) are presented in Fig. 14. The maxima of {220} and {200} in the center of the pole figures of wuestite and {220} of magnetite represent the well known ⟨110⟩- and ⟨100⟩-fiber textures of cubic minerals and metals (see e.g. Siemes et al., 1994). The ⟨110⟩- and ⟨100⟩-fiber textures were measured recently in compression tests on magnesiowüstite by Heidelbach et al. (2001) at temperatures between 725 and 1125 °C. Experimental deformation of magnetite at temperatures up to 300 °C (Müller and Siemes, 1972) also resulted in the ⟨110⟩ fiber texture. The weak maximum in the center of the {111}-magnetite pole figures of the S-samples could be interpreted as result of a topotactical transformation of the (001) maximum of hematite to the {111} maximum of magnetite preserving the close packed oxygen planes (Wagner et al., 1977). Not all measured pole figures of magnetite and wuestite are as distinct as in Fig. 14a for wuestite.

Experiments where oxygen diffuses into iron show the same reactions to oxides as we observed. Kim and Szpunar (2001) investigated the grain growth of wuestite, magnetite and hematite in oxidation experiments on steel. Wuestite develops a columnar grain structure and magnetite a simple

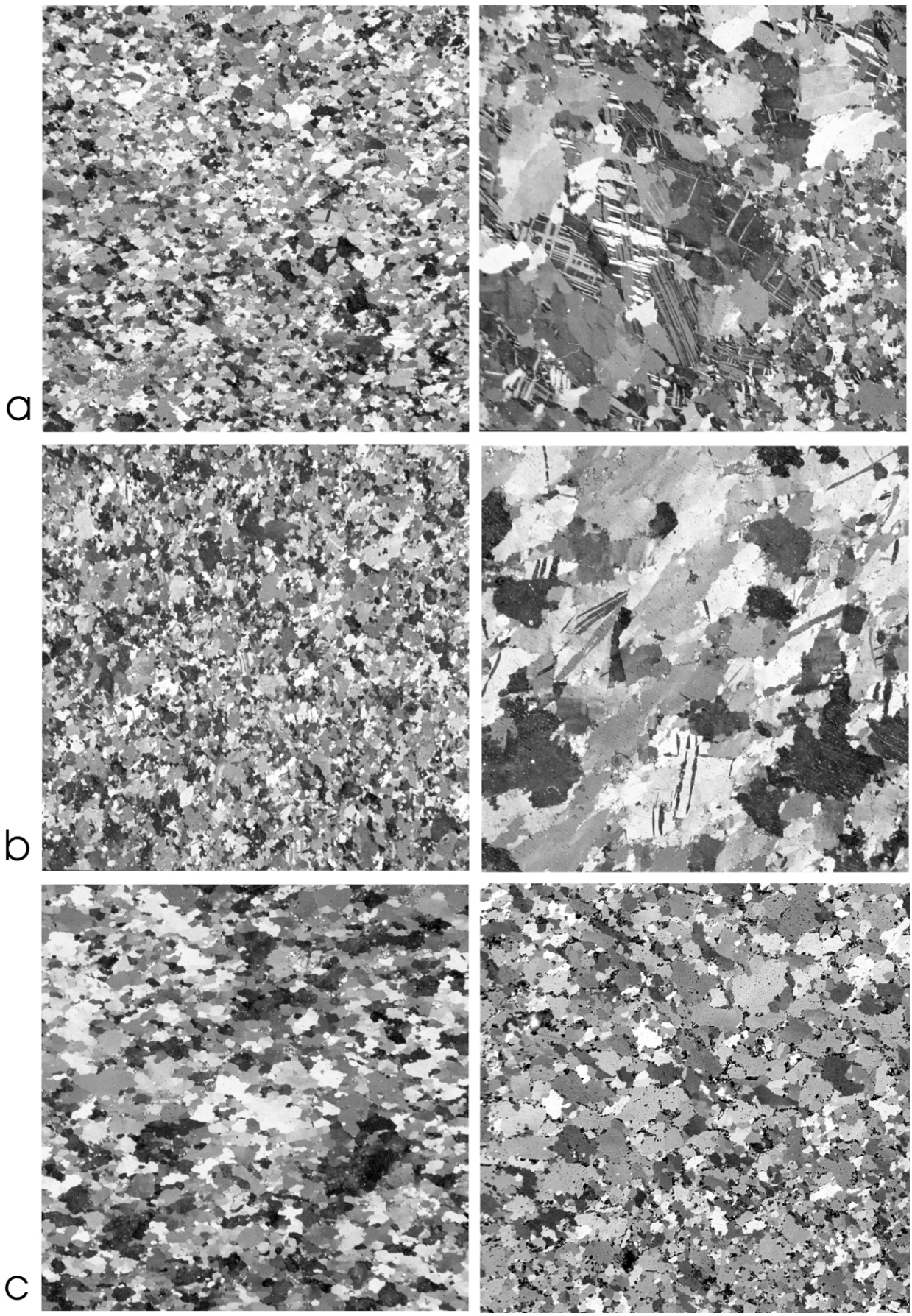
a
b
c

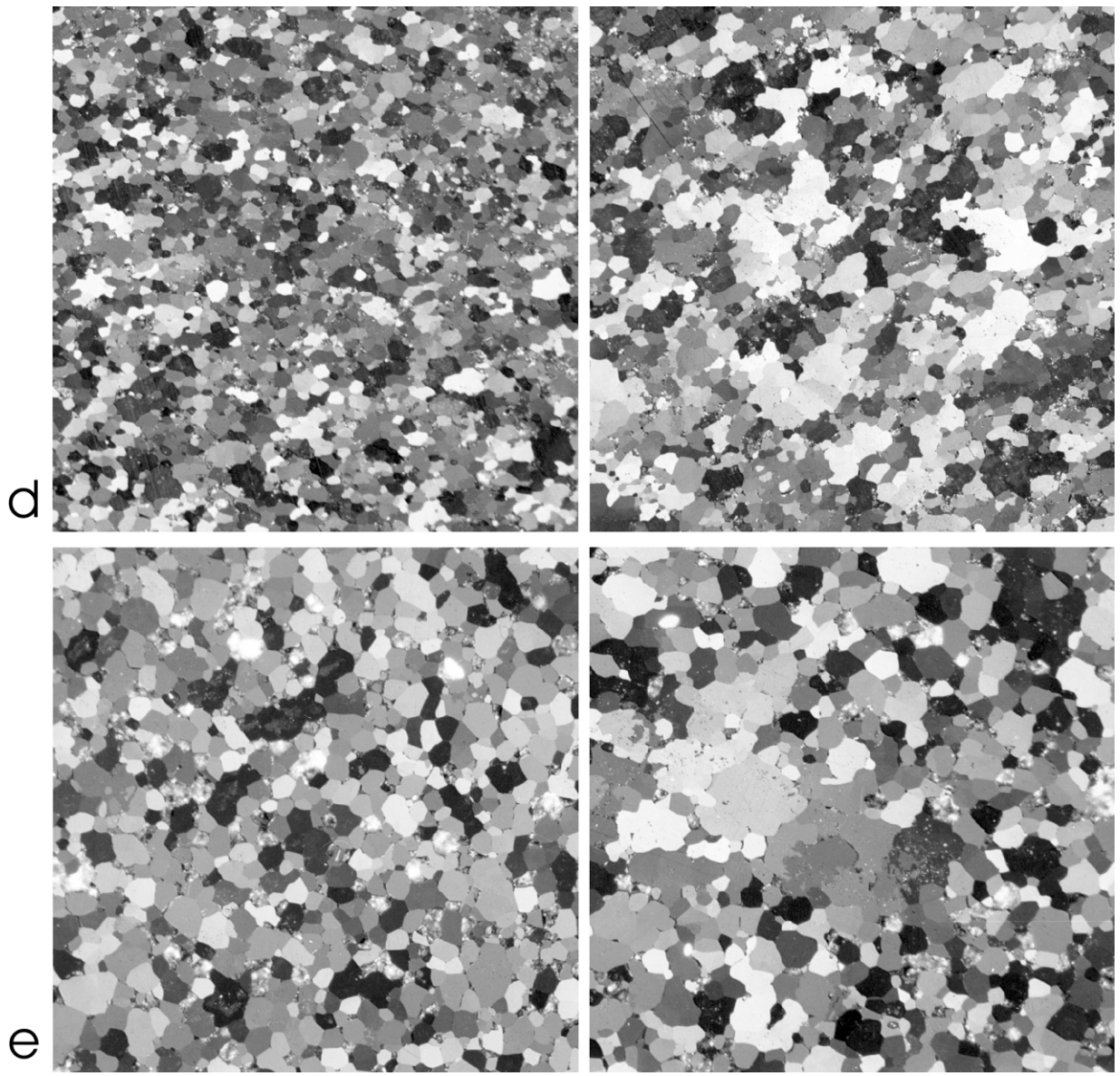

Fig. 12 (*continued*)

structure of rounded grains, but both with a distinct {100} fiber texture with the fiber axis parallel to the columns and perpendicular to the boundaries between the different phases.

5. Geological relevance and conclusions

In order to understand natural processes the laboratory data have to be extrapolated to geological conditions with strain rates of 10^{-10} to 10^{-14} s^{-1} at temperatures up to 600–700 °C, which results in significantly lower strengths of the material. The problems of extrapolation are discussed in detail by Paterson (1976, 1987, 2001).

5.1. Natural and experimental textures of hematite

All textures of hematite ores from quite different origins

Fig. 12. Photomicrographs of the hematite ore from Sishen Mine after experimental deformation, $\dot{\epsilon} = 10^{-4}$ s^{-1}, 300 MPa. Polished sections perpendicular to the foliation, σ_1 top to bottom, 87° XPL, width of view 600 μm: (a) N02, 700 °C, $\epsilon = 14.5\%$, left: fine grains, right: slightly coarser grains with two sets of r–t twin lamellae, (b) N04, 800 °C, $\epsilon = 21.0\%$, left: fine grains, right: coarse grains with a few twin lamellae, (c) N05, 900 °C, $\epsilon = 20.5\%$, left: finer grains, right: coarser grains with undulose extinction, (d) N03, 1000 °C, $\epsilon = 20.9\%$, onset of dynamic recrystallization, left: finer grains, right: coarser grains, (e) N06, 1100 °C, $\epsilon = 20.4\%$, dynamic recrystallized foam structure, left: finer grains, right: coarser grains.

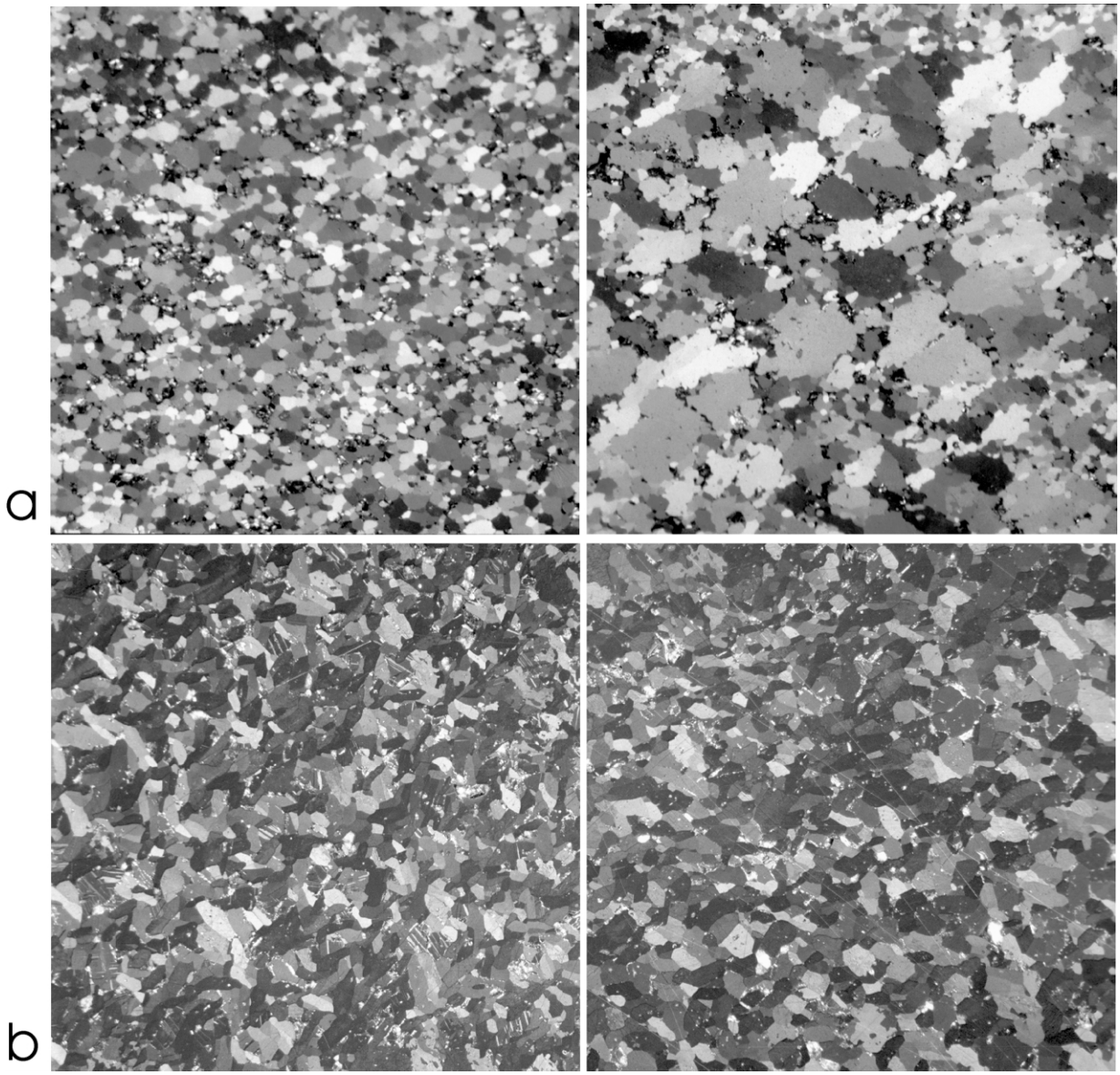

Fig. 13. Photomicrographs of the hematite ore from Sishen Mine (S) and Mutuca Mine (R) after experimental deformation. Polished sections perpendicular to the foliation, σ_1 top to bottom, 87° XPL, width of view 600 μm: (a) S06, 900 °C, $\epsilon = 20.5\%$, $\dot{\epsilon} = 10^{-5}\ s^{-1}$, left: finer grains, right: coarser grains, (b) left: R20, 600 °C, $\epsilon = 7.1\%$, $\dot{\epsilon} = 10^{-6}\ s^{-1}$, right: R22, 700 °C, $\epsilon = 8.3\%$, $\dot{\epsilon} = 10^{-6}\ s^{-1}$.

(e.g. Neff and Paulitsch, 1960; Paulitsch et al., 1967; Attewell and Taylor, 1969; Esling et al., 1981; Quade and Walde, 1982; Hrouda et al., 1985; Höfler et al., 1986; Will et al., 1990; Rosière et al., 1996, 1998, 2001; Quade et al., 2000) show that the pole of the foliation coincides with the maximum of the basal plane. Therefore, one of the most interesting results in the light of interpretation of naturally deformed hematite ores is the strong influence of the c(001) a⟨110⟩ slip mode at temperatures between 800 and 900 °C for the formation of the experimental textures. Variation of the degree of preferred orientation, the presence of distinct pole figures (single maxima and single girdles) in samples related to distinct structures and with different anisotropy of magnetic susceptibility indicate the sensitivity of crystallographic preferred orientation and to differences in the intensity and type of finite strain.

The naturally deformed iron ores of the Iron Quadrangle, Minas Gerais, Brazil, underwent a maximum temperature of 600 °C (e.g. Pires, 1995), a temperature at which this laboratory work started. It can be expected that extrapolation of the laboratory data to geological strain rates leads to lower temperatures where basal slip strongly influences the formation of deformation textures. The critical resolved shear stress of the basal slip systems has to be determined by deformation experiments on single crystals. Hematite ores with a high degree of preferred orientation and presenting a foam structure (Fig. 12e) are known from deposits of the Iron Quadrangle, and ores with an intensely developed

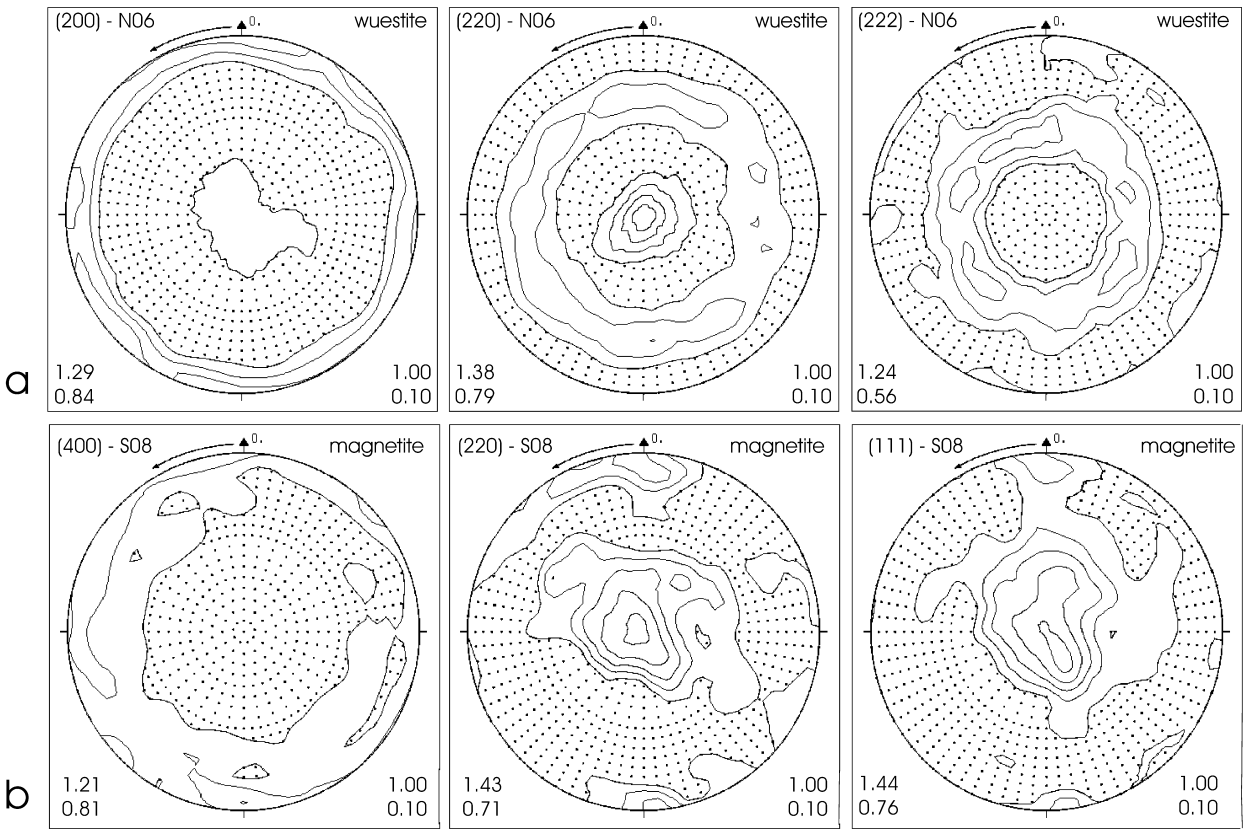

Fig. 14. Pole figures of wuestite (a) from the reaction rim of specimen N06 after deformation at 1100 °C, $\epsilon = 20.4\%$, $\dot{\epsilon} = 10^{-4}\ s^{-1}$. and magnetite (b) from the reaction rim of specimen S08 after deformation at 1000 °C, $\epsilon = 20.0\%$, $\dot{\epsilon} = 10^{-5}\ s^{-1}$.

schistosity (e.g. Rosière et al., 2001), characterized by the parallel orientation of platy hematite crystals (specularite), are another common type.

The coaxial deformation experiments reveal the influence of an initial preferred orientation on the newly developed texture. Besides the rather dramatic change of the prism patterns in Figs. 8 and 9 there is also a weak tendency for the basal plane to reorient perpendicular to the compression axis. This is certainly consistent with the observed naturally formed hematite textures. Under the assumed simple shear formation of the schistose ores one would expect from the operating c(001) a⟨110⟩ glide mode only an a-prism maximum centered on the lineation, but the textures of naturally formed hematite ores always show all the prism maxima centered on the lineation. Deformation of hematite by simple shear experiments (Paterson and Olgaard, 2000) could help to understand the formation of these natural hematite textures much better.

5.2. Flow strengths of the minerals of hematite ores at geological strain rates

The iron ores of the Iron Quadrangle are classified according to their composition as hematite ores (with Fe-content greater than 63 wt%), quartz bearing itabirite ores (with Fe-content between 35 and 63 wt%) and carbonate (calcite and dolomite) bearing ores (dolomite itabirite). The flow laws for intracrystalline plasticity of quartz, calcite, dolomite, and hematite are used to extrapolate the strengths of these four minerals to the geological relevant strain rate of $10^{-14}\ s^{-1}$ (Fig. 15).

5.2.1. Flow strength of quartz

The dark shaded band in Fig. 15 indicates the range of flow strengths for intracrystalline plasticity of synthetic quartz according to Paterson and Luan (1990, fig. 2). The lighter shaded area indicates the upper bound of flow data from Brodie and Rutter (2000) for hot pressed Brazilian quartz. The data for these flow laws are acquired at confining pressures of 300 MPa. With increasing confining pressure and water content quartz shows a clear trend of decreasing strength (e.g. Kronenberg and Tullis, 1984).

5.2.2. Flow strength of calcite

Early experimental studies on the flow strength of marbles (Heard and Raleigh, 1972; Schmid et al., 1980) and extrapolation of the laboratory data to strain rates of $10^{-14}\ s^{-1}$ show that the strengths of marbles with grain sizes between 200 and 500 μm are mostly positioned within the range of the strength of quartz. Only the strength of Solnhofen Limestone (Schmid et al., 1977) with a grain size of 4 μm is much lower than that of quartz. Experiments on fine-grained synthetic calcite rocks by Walker et al. (1990) revealed that the flow strength of calcite is grain size

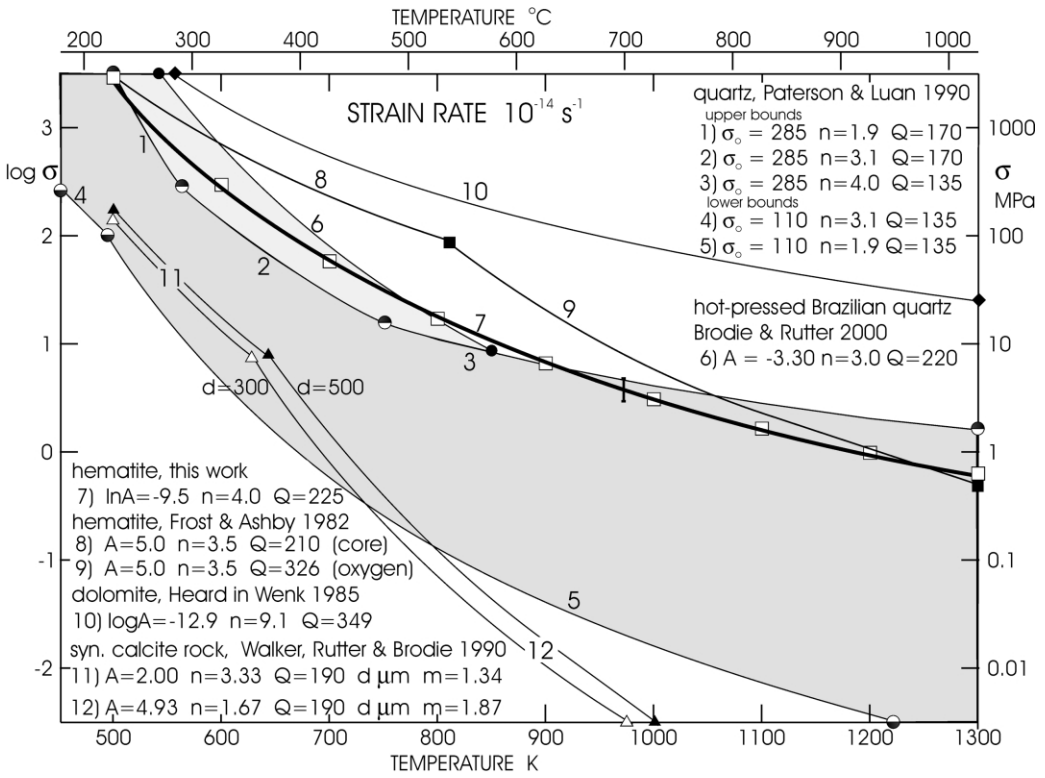

Fig. 15. Strength of hematite, quartz, dolomite and calcite at a strain rate of 10^{-14} s^{-1} in the temperature range between 200 and 1000 °C calculated from the indicated flow laws with $\dot{\epsilon} = A\sigma^n d^{-m}\exp(-Q/RT)$ where $\dot{\epsilon}$ is strain rate (s^{-1}), A is a pre-exponential constant (MPa^{-n} s^{-1}), σ is stress (MPa), Q is the activation energy (kJ mol^{-1}), T is temperature (K), R is the gas constant, n the stress exponent, d is the grain size (µm) and m the grain size exponent. Experimental error $\Delta\log\sigma = \pm$ 0.27 for hematite at 700 °C is indicated.

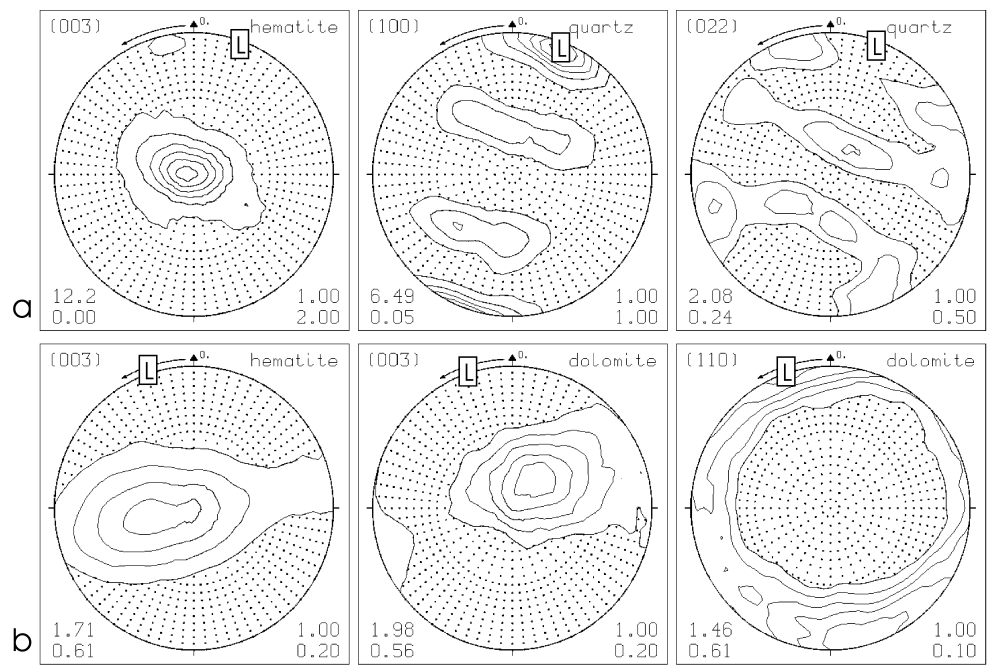

Fig. 16. Neutron pole figures of hematite ores, equal area projections parallel to the foliation, L indicates the lineation. (a) Hematite–quartz ore from Fire Lake, Newfoundland/Quebec, Canada. The (003)-pole figure of hematite and the (100)- and (011/101)-pole figures of quartz show the same relation to the lineation and foliation as the high-grade ores. (b) Hematite–dolomite ore from Águas Claras, Iron Quadrangle, Brazil. The (003)-pole figure of hematite and the (003)- and (110)-pole figures of dolomite display slightly different orientations.

sensitive and the strengths of calcite rocks can be described by a power law equation of the form: $\dot{\epsilon} = A\sigma^n d^{-m}\exp(-Q/RT)$ where d (μm) is the grain size and m the grain size exponent. According to this equation strength of calcite was calculated (Walker et al., 1990) for a grain size of $d = 300$ and 500 μm and $m = 1.34$ and 1.87 for lower and higher temperatures, respectively (Fig. 15). This grain size interval of 300–500 μm is typical for carbonitic iron ores and the calculations reveal that the calcite strengths are within the range or below those of quartz. In recently published conference proceedings (e.g. de Bresser et al., 2001) it is reported that in order to predict the strength of calcite rocks under natural conditions not only the grain size but further parameters such as dispersed phases and impurities in solid solution must be considered.

5.2.3. Flow strength of dolomite

The most recently described deformation experiments on Crevola dolomite with a grain size of 700 μm are presented by Barber et al. (1994). At a strain rate of $10^{-6}\,s^{-1}$ and 900 °C this dolomite reveals a strength of 305 MPa. Under nearly the same conditions, hematite (this study; 120 MPa), quartzite (e.g. Paterson and Luan, 1990; 220 MPa), and marble (e.g. Schmid et al., 1980; 12 MPa) are distinctly weaker. Power flow law data were derived from experiments on the same Crevola dolomite (Heard, 1985). The predicted strengths under geological conditions (Fig. 15) are much higher than the strengths of hematite and quartz. This finding is in contradiction to the field observations, because hematite and dolomite often behave very similarly during natural deformation.

5.2.4. Flow strength of hematite

The flow strengths of hematite calculated from the flow law of this work are mostly positioned within the upper range of the quartz strengths (Fig. 15). This corresponds with the field observations. The strength data of hematite calculated from the flow laws given by Frost and Ashby (1982), based on the experimental data of Crouch and Pascoe (Section 2) are above our strength data. The differences are attributed to the different experimental deformation techniques without applying confining pressure and due to the quite different synthetic porous material used.

5.3. Understanding competence contrasts in banded iron formations from field observations

Banded iron ores often show characteristic alternating layers of hematite and quartz or hematite and carbonates on a centimeter to millimeter scale. These ores are very suitable for measuring preferred orientation of all minerals on one and the same specimen in their original position by means of neutron diffraction. This permits the study of the texture development of hematite, quartz and carbonates at certain geological strain rates and environmental conditions (e.g. temperature, confining pressure, availability of fluids) during a metamorphic cycle.

Fig. 16a shows, as an example, pole figures of hematite and quartz and Fig. 16b of hematite and dolomite. Hematite in both quartzitic and dolomitic ores always shows the same pole figure patterns as in the pure high-grade hematite ore (Fig. 1) and is usually strongly related to the macroscopic foliation and lineation. The pole figures of gangue minerals of both samples show, in a similar way, a close relation to the macroscopic foliation and lineation. It is therefore reasonable to assume similar tectonic constraints with either simultaneous formation of the texture under conditions that allowed the flow of both minerals at the same time, or formation of the texture at different times of one mineral after another under suitable conditions for each of them. However, the wide variation of the pole figure patterns of each mineral, especially in relation to the lineation can be attributed to differences in their flow behavior according to the prevailing conditions, permitting an accommodation of the texture of the most ductile mineral and preserving the old textural imprints of the less ductile phase. Neutron texture analyses of quartz–itabiritic and dolomitic ores are recent subjects of thorough further studies (Siemes et al. 2002).

These experiments furnish results that allow a more consistent interpretation of structures both in outcrops and on a microscopic scale of samples from different metamorphic domains. A strong contrast in the rheological behavior of individual layers of the ores is commonly noticeable. This is due to the activation of different mechanisms probably during different stages of the deformational history (e.g. Lagoeiro 1999), although in several areas a more homogeneous behavior in the ore layers can be observed. This apparent discrepancy is due to variations in the internal and external factors that control the rheology of the minerals such as grain size, mineralogy, strain rate etc.

Hippertt et al. (2001) report deformation partitioning between quartz and hematite during folding of Brazilian banded iron formations (itabirites). The preferentially brittle behavior of hematite and fluid assisted processes active during the deformation of quartz and calcite as described by these authors suggest, for instance, faster strain rates and/or lower temperatures than those that are responsible for the formation of the described natural deformed textures of hematite.

Acknowledgements

This work was supported by the German Science Foundation (DFG, Si/209-27) and benefited from the cooperation with C.A. Rosière, Belo Horizonte and H. Quade, Clausthal in the frame of the PROBRAL (CAPES/DAAD) project: ‘Texture, physical anisotropy and metallurgy of iron ores of the Iron Quadrangle (Minas

Gerais, Brazil)'. Ch. Hennig-Michaeli traveled in 1990 to Canberra to run the preliminary tests at the laboratory of M.S. Paterson, her contribution to this work is gratefully acknowledged. Thanks are due to H.-G. Brokmeier and E.M. Jansen of the Forschungszentrum Geesthacht for the neutron measurements of the hematite textures of ore samples from the Iron Quadrangle (Fig. 1) in the course of the PROBRAL project. We kindly thank the reviewers, especially Alan Boyle, Liverpool, for their critical remarks and improvements. The staff of the Mineralogical Institute of the RWTH Aachen particularly M. Brand, T. Derichs, W. Grawinkel, G. Paprotny, G. Siebel, M. Wiechert, and A. Wiechowski contributed with a variety of preparations and measurements.

References

Atkinson, B.K., 1977. The kinetics of ore deformation: its illustration and analysis by means of deformation-mechanism maps. Geologiska Föreningens Förhandlingar 99, 186–197.

Attewell, P.B., Taylor, R.K., 1969. A microtextural interpretation of a Welsh slate. International Journal of Rock Mechanics and Mining Sciences 6, 423–438.

Barber, D.J., Wenk, H.-R., Heard, H.C., 1994. The plastic deformation of polycrystalline dolomite: comparison of experimental results with theoretical predictions. Materials Science Engineering A175, 83–104.

Beukes, N.J., 1986. The Transvaal Sequence in Griqualand West. In: Anhaeuser, C.R., Maske, S. (Eds.), Mineral Deposits of Southern Africa, Geological Society of South Africa, Johannesburg, pp. 819–828.

de Bresser, H., Evans, B., Renner, J., 2001. Predicting the strength of calcite rocks under natural conditions. Deformation Mechanisms, Rheology and Tectonics meeting Noordwijkerhout, Netherlands, Abstracts, p. 31.

Brodie, K.H., Rutter, E.H., 2000. Deformation mechanisms and rheology: why marble is weaker than quartzite. Journal of the Geological Society of London 157, 1093–1096.

Brokmeier, H.-G., 1994. Application of neutron diffraction to measure preferred orientations of geological materials. In: Bunge, H.-J., Skrotzki, W., Siegesmund, S., Weber, K. (Eds.), Textures of Geological Materials. Deutsche Gesellschaft für Materialwissenschaften, Informationsgesellschaft, Oberursel, pp. 327–344.

Brokmeier, H.-G., 1999. Advantages and applications of neutron texture analysis. Textures and Microstructures 33, 13–34.

Brokmeier, H.-G., Zink, U., Schnieber, R., Witassek, B., 1998. TEX-2, Texture analysis at GKSS Research Center (instrumentation and application). In: Schwarzer, R. (Ed.), Texture and Anisotropy of Polycrystals. Materials Science Forum 273–275, 277–282.

Bunge, H.-J., 1989. Advantages of neutron diffraction in texture analysis. Textures and Microstructures 10, 265–307.

Chang, R.H., Wagner, J.B. Jr, 1972. Direct-current conductivity and iron tracer diffusion in hematite at high temperatures. Journal of the American Ceramic Society 55, 211–213.

Charpentíer, Ph., Rabbe, P., Manenc, J., 1968. Mise en évidence de la plasticité de la magnétite mesure de la dureté en fonction de la témperature. Materials Research Bulletin 3, 69–78.

Crouch, A.G., 1972. High-temperature deformation of polycrystalline Fe_2O_3. Journal of the American Ceramic Society 55, 558–563.

Crouch, A.G., 1973. Tensile creep of Fe_2O_3. Transactions of the British Ceramic Society 72, 307–311.

Esling, C., Quade, H., Wagner, F., Walde, R., 1981. Pesquisa textural de minério hematítico da jazida de Águas Claras (MG) pelo método de difraçãco de nêutrons. Revista Brasileira de Geociências 11, 84–90.

Fischer, B., Helmich, R., 1981. Zum Einfluβ von Phosphatglas auf die Warmfestigkeit von Palladium. Wissenschaftliche Zeitschrift der Friedich-Schiller-Univiversität Jena. Mathematisch-Naturwissenschaftliche Reihe 30, 921–925.

Frost, H.J., Ashby, M.F., 1982. Deformation-Mechanism-Maps. The Plasticity and Creep of Metals and Ceramics, Pergamon Press, Oxford.

Heard, H.C., 1985. Personal communication, Crevola dolomite, table 2, p. 368. In: Wenk, H.-R., (Ed.), Preferred Orientation in Deformed Metals and Rocks, an Introduction to Modern Texture Analysis, Academic Press, Orlando, p. 610.

Heard, H.C., Raleigh, C.B., 1972. Steady-state flow in marble at 500 to 800 °C. Geological Society of America Bulletin 83, 935–956.

Heidelbach, F., Stretton, I., Mackwell, S., 2001. Microtextures and misorientation characteristics of subgrain rotation crystallization in magnesiowuestite $(Mg_{.8}Fe_{.2})O$ experimentally deformed by dislocation creep. Deformation Mechanisms, Rheology and Tectonics meeting Noordwijkerhout, Netherlands, Abstracts, p. 66.

Hennig-Michaeli, C., 1977. Microscopic structure studies of experimentally and naturally deformed hematite ores. Tectonophysics 39, 255–271.

Hennig-Michaeli, C., Siemes, H., 1982. Experimental deformation of hematite crystals between 25 °C and 400 °C at 400 MPa confining pressure. In: Schreyer, W., (Ed.), High Pressure Researches in Geoscience, E. Schweizerbart, Stuttgart, pp. 133–150.

Heuer, A.H., Tighe, N.J., Cannon, R.M., 1980. Plastic deformation of fine-grained alumina (Al_2O_3), basal slip and nonaccomodated grain-boundary sliding. Journal of the American Ceramic Society 63, 53–57.

Hippertt, J., Lana, C., Takeshita, T., 2001. Deformation partitioning during folding of banded iron formation. Journal of Structural Geology 23, 819–834.

Hirose, K., Kawamoto, T., 1995. Hydrous partial melting of lherzolite at 1 GPa: the effect of H_2O on the genesis of basaltic magmas. Earth and Planetary Science Letters 133, 463–472.

Höfler, S., Schäfer, W., Will, G., 1986. Texture measurements at the neutron diffractometer in Jülich. In: Bunge, H.J., (Ed.), Experimental Techniques of Texture Analysis, Deutsche Gesellschaft für Materialwissenschaften, Informationsgesellschaft Oberursel, pp. 241–251.

Hrouda, F., Siemes, H., Herres, N., Hennig-Michaeli, C., 1985. The relationship between the magnetic anisotropy and the c-axis fabric in a massive hematite ore. Journal of Geophysics 65, 174–182.

Jansen, E., Schaefer, W., Kirfel, A., 2000. The Juelich neutron diffractometer and data processing in rock texture investigations. Journal of Structural Geology 22, 1559–1564.

Kawamoto, T., Hirose, K., 1994. Au–Pd sample containers for melting experiments on iron and water bearing systems. European Journal of Mineralogy 6, 381–385.

Kim, B.-K., Szpunar, J.A., 2001. Grain growth of iron oxides during high temperature oxidation. In: Gottstein, G., Molodov, D.A. (Eds.), Recrystallization and Grain Growth, Proceedings of the First Joint International Conference, Springer Verlag, Berlin, pp. 489–494.

Kollenberg, W., 1986. Microhardness measurement on haematite crystals at temperatures up to 900 °C. Journal of Material Science 21, 4310–4314.

Kronenberg, A.K., Tullis, J., 1984. Flow strengths of quartz aggregates: grain size and pressure effects due to hydrolytic weakening. Journal of Geophysical Research 89, 4298–4312.

Lagoeiro, L., 1999. Contrasting c-axis fabric patterns in layers of different proportion of quartz and iron oxides. In: Szpunar, J.A. (Ed.), Proceedings of the Twelfth International Conference on Textures of Materials (ICOTOM-12), NRC Research Press, Ottawa, Canada, Vol. 2, pp. 1528–1533.

Müller, P., Siemes, H., 1972. Zur Festigkeit und Gefügeregelung von experimentell verformten Magnetiterzen. Neues Jahrbuch für Mineralogie, Abhandlungen 117, 39–60.

Neff, H., Paulitsch, P., 1960. Röntgenographische Bestimmung der Hämatitregel in natürlichen Gefügen. Neues Jahrbuch für Mineralogie, Abhandlungen 94, 1401–1410.

Pascoe, R.T., 1974. A stress relaxation technique for oxides. Transactions of the British Ceramic Society 73, 143–146.

Paterson, M.S., 1970. A high pressure, high-temperature apparatus for rock deformation. International Journal of Rock Mechanics and Mining Sciences 7, 517–526.

Paterson, M.S., 1976. Some current aspects of experimental rock deformation. Philosophical Transactions of the Royal Society of London A283, 163–172.

Paterson, M.S., 1987. Problems in the extrapolation of laboratory rheological data. Tectonophysics 133, 33–43.

Paterson, M.S., 1990. Rock deformation experimentation. In: Duba, A.G., Durham, W.B., Handin, J.W., Wang, H.F. (Eds.), The Brittle–Ductile Transition in Rocks. The Heard Volume, American Geophysical Union Geophysical Monograph 56, pp. 187–194.

Paterson, M.S., 2001. Relating experimental and geological rheology. International Journal of Earth Sciences (Geologische Rundschau) 90, 157–167.

Paterson, M.S., Luan, F.C., 1990. Quartzite rheology under geological conditions. In: Knipe, R.J., Rutter, E.H. (Eds.), Deformation Mechanisms, Rheology and Tectonics. Geological Society Special Publication 54, pp. 299–307.

Paterson, M.S., Olgaard, D.L., 2000. Rock deformation tests to large shear strains in torsion. Journal of Structural Geology 22, 1341–1358.

Paulitsch, P., Schicht, R., Mons, W., 1967. Zur Gefügeregelung von Hämatit. Die Naturwissenschaften 54 (4), 88.

Pires, F.R.M., 1995. Textural and mineralogical variations during metamorphism of the Proterozoic Itabira Iron Formation in the Quadrilátero Ferrífero, Minas Gerais, Brazil. Anais da Academia Brasileira de Ciência 67, 77–105.

Quade, H., Walde, R., 1982. Texturuntersuchungen an hämatitischen Reicherzen. Archiv für das Eisenhüttenwesen 53, 85–89.

Quade, H., Rosière, C.A., Siemes, H., Brokmeier, H.-G., 2000. Fabrics and textures of Precambrian iron ores from Brazilian deposits. Zeitschrift für angewandte Geologie, Sonderheft 1, 155–162.

Rosière, C.A., Quade, H., Siemes, H., Chemale, F. Jr, Resende de Souzam, E.M., 1996. Um Modelo para a Evolução Microestrutural dos Minérios de Ferro do Quadrilátero Ferrífero. Parte II-Trama, Textura e Anisotropia de Susceptibilidade Magnética. Geonomos 4, 61–75.

Rosière, C.A., Quade, H., Siemes, H., Chemale, F. Jr, 1998. Fabric, texture and anisotropy of magnetic susceptibility in high-grade iron ores from the Quadrilátero Ferrífero, Minas Gerais, Brazil. Materials Science Forum 273-275, 693–700.

Rosière, C.A., Siemes, H., Quade, H., Brokmeier, H.-G., Jansen, E.M., 2001. Microstructures, textures and deformation mechanisms in hematite. Journal of Structural Geology 23, 1429–1440.

Schaeben, H., 1994. Diskrete mathematische Methoden zur Berechnung und Interpretation von kristallographischen Orientierungsdichten. Deutsche Gesellschaft für Materialwissenschaften, Informationsgesellschaft mbH, Oberursel.

Schaeben, H., Siemes, H., 1996. Determination and interpretation of preferred orientation with texture goniometry: an application of indicators to maximum entropy pole- to orientation-density inversion. Mathematical Geology 28, 169–201.

Schmid, S.M., Boland, J.N., Paterson, M.S., 1977. Superplastic flow in fine-grained limestone. Tectonophysics 43, 257–291.

Schmid, S.M., Paterson, M.S., Boland, J.N., 1980. High temperature flow and dynamic recrystallization in Carrara marble. Tectonophysics 65, 245–280.

Siemes, H., Hennig-Michaeli, C., 1985. Ore minerals. In: Wenk, H.-R., (Ed.), Preferred Orientation in Deformed Metals and Rocks, an Introduction to Modern Texture Analysis, Academic Press, Orlando, pp. 335–360.

Siemes, H., Jansen, E.M., Niederschlag, E., 1994. Crystallographic preferred orientation of experimentally deformed sulfide ores. In: Bunge, H.J., Siegesmund, S., Skrotzki, W., Weber, K. (Eds.), Textures of Geological Materials, Deutsche Gesellschaft für Materialwissenschaften, Informationsgesellschaft, Oberursel, pp. 231–250.

Siemes, H., Schaeben, H., Rosière, C.A., Quade, H., 2000. Crystallographic and magnetic preferred orientation of hematite in banded iron ores. Journal of Structural Geology 22, 1747–1759.

Siemes, H., Günther, A., Rosière, C.A., Quade, H., 2002. Deformation partitioning and textures of banded iron ores. In: Robb, L., Montjoie, R. (Eds.), Extended Abstracts (CD-ROM), 11th Quadrennial IAGOD Symposium and Geocongress 2002, Windhoek, Namibia, Geological Survey of Namibia.

Sotin, C., Poirier, J.P., 1984. Analysis of high-temperature creep experiments by generalized nonlinear inversion. Mechanics of Materials 3, 311–317.

Stevenson, M.E., Kaji, M., Bradt, R.C., 2002. Microhardness anisotropy and the indentation size effect on the basal plane of single crystal hematite. Journal of the European Ceramic Society 22, 1137–1148.

Traas, C., Siemes, H., Schaeben, H., 1994. Smoothing pole figures using tensor products of trigonometric and polynomial splines. Materials Science Forum 157–162, 453–458.

Veit, K., 1922. Künstliche Schiebungen und Translationen in Mineralien. Neues Jahrbuch für Mineralogie, Geologie und Paläontologie, Beilage-Band 45, 121–148.

Wagner, F., Esling, C., Baro, R., Englander, M., 1977. Textures of iron oxides by neutron diffration and topotactical relation. Zeitschrift für Metallkunde 68, 701–704.

Walker, A.N., Rutter, E.H., Brodie, K.H., 1990. Experimental study of grain size sensitive flow of synthetic, hot-pressed calcite rocks. In: Knipe, R.J., Rutter, E.H. (Eds.), Deformation Mechanisms, Rheology and Tectonics. Geological Society Special Publication 54, pp. 259–284.

Wenk, H.-R., 1998. Typical textures in geological materials and ceramics. In: Kocks, U.F., Tomé, C.N., Wenk, H.-R. (Eds.), Texture and Anisotropy, Cambridge University Press, Cambridge, pp. 240–280.

Will, G., Merz, P., Schäfer, W., Dahms, M., 1990. Application of position sensitive detectors for neutron diffraction texture analysis of hematite ore. In: Barret, C.S., Gilfrisch, J.V., Huang, T.C., Jenkins, R., Predecki, P.K. (Eds.), Advances in X-Ray Analysis 33, Plenum Press, New York, pp. 277–283.